Production of polarized vector mesons off nuclei

B. Z. Kopeliovich,[1,2] J. Nemchik,[3] and Ivan Schmidt[1]
[1]*Departamento de Física y Centro de Estudios Subatómicos, Universidad Técnica Federico Santa María, Valparaíso, Chile*
[2]*Joint Institute for Nuclear Research, Dubna, RU-141980 Moscow Region, Russia*
[3]*Institute of Experimental Physics SAS, Watsonova 47, SK-04001 Kosice, Slovakia*
(Received 13 March 2007; published 20 August 2007)

Using the light-cone QCD dipole formalism we investigate manifestations of color transparency (CT) and coherence length (CL) effects in electroproduction of longitudinally (L) and transversally (T) polarized vector mesons. Motivated by forthcoming data from the HERMES experiment we predict both the A and Q^2 dependence of the L/T ratios for ρ^0 mesons produced coherently and incoherently off nuclei. For an incoherent reaction the CT and CL effects add up and result in a monotonic A dependence of the L/T ratio at different values of Q^2. In contrast, for a coherent process the contraction of the CL with Q^2 causes an effect opposite to that of CT and we expect quite a nontrivial A dependence.

DOI: 10.1103/PhysRevC.76.025210 PACS number(s): 13.60.Le, 12.38.−t, 13.85.Lg, 24.85.+p

I. INTRODUCTION

Electroproduction of vector mesons has been intensively studied during the past three decades. Numerous fixed-target experiments have provided high-quality data: the OMEGA [1] and NMC [2] experiments at CERN, CHIO [3] and E665 experiments at Fermilab [4], etc. [5]. In particular, the E665 Collaboration [6] observed for the first time a manifestation of color transparency [7,8] in vector meson production on nuclear targets. The data confirmed the predictions for color transparency presented in Ref. [9].

Moreover, important dynamical information on vector meson electroproduction, in a wide range of Q^2 and energies and for different photon polarizations, transverse (T) and longitudinal (L), was provided by experiments performed by both the ZEUS [10] and H1 [11] Collaborations at HERA. In particular it was found that the longitudinal-to-transverse ratio, R_{LT}, for exclusive electroproduction of ρ^0 mesons, rises with Q^2, but has a weak energy dependence at fixed Q^2 [2,4,12–21]. Some correlation between the energy and Q^2 dependence was detected in the ZEUS experiment [12]. The energy dependence of the ratio R_{LT} is stronger at larger Q^2.

These observations can be understood within the dipole approach [22]. The shrinkage of the $\bar{q}q$ component of the photon with Q^2 and the small-size behavior of the dipole cross section [7], $\sigma_{\bar{q}q}(r) \sim r^2$,[1] lead to a *scanning effect* [9,22,23]. Namely, the vector meson production amplitude is dominated by the contribution of dipole sizes of the order of $r \sim r_S$, where

$$r_S \approx \frac{Y}{\sqrt{Q^2 + m_V^2}}, \tag{1}$$

and the product of the photon wave function and the dipole cross section forms a sharp peak. Varying Q^2 and the mass of vector meson m_V one can study the transition from the nonperturbative region of large r_S to the perturbative region of very small $r_S \ll R_V$, where R_V is the radius of the vector meson.

Factor Y in Eq. (1) was evaluated in [22] at $Y \approx 6$. However, this estimate made use of a nonrelativistic approximation, which is reasonable for charmonium and is rather accurate for bottonium production. Moreover, in the general case the parameter Y depends on polarization and increases slowly with Q^2. The Q^2 dependence of $Y_{T,L}$ is related to so-called aligned-jet configurations of the $\bar{q}q$ configurations when q or $\bar{q}$ carry almost the whole momentum of the photon. Since these end-point configurations in longitudinally polarized photons are suppressed, one should expect $Y_L < Y_T$. In another words, the production amplitude of longitudinal vector mesons scans their wave function at smaller transverse sizes. According to Eq. (1) higher Q^2 results in a smaller transverse size of the color $\bar{q}q$ dipole (i.e., in a smaller r_S). Stronger energy dependence of the dipole cross section $\sigma_{\bar{q}q}(r, s)$ at smaller dipole size causes a weak energy dependence of the ratio R_{LT} (see also Ref. [24]). However, large errors of available data do not allow this energy dependence to be seen clearly.

Equation (1) shows that one can reach small perturbative scanning radius only at very large scale ($Q^2 \gg m_V^2$).

There is much experimental and theoretical evidence [25,26] that a semihard scale of a nonperturbative origin exists in QCD [27]. Namely, the mean transverse distance of gluon propagation is small, of the order of $r_0 \sim 0.3$ fm. To rely on pQCD calculations one should make the scanning radius smaller than r_0, that is,

$$\left(Q^2 + m_V^2\right) \gtrsim Q^2_{\mathrm{pQCD}} = \frac{Y^2}{r_0^2}. \tag{2}$$

As was discussed in Refs. [28–30], nuclear targets represent unique analyzers of the dynamics of vector meson production. They allow us to study other phenomena such as color transparency (CT), coherence length (CL) effects, and gluon shadowing (GS). These effects were studied in Ref. [28] for coherent and incoherent electroproduction of vector mesons, and within a quantum-mechanical description of the $\bar{q}q$

[1] $\sigma_{\bar{q}q}(r)$ is the cross section for the interaction with a nucleon of the $\bar{q}q$ fluctuations of the photon having transverse separations $\vec{r}$.

evolution, based on the light-cone (LC) Green function technique [31]. The same LC Green function formalism has been applied also for Drell-Yan production in proton-nucleus and nucleus-nucleus interactions [32], and for nuclear shadowing in deep-inelastic scattering [33,34].

Data for vector meson production off nuclei are usually presented in the form of the so-called nuclear transparency, defined as a ratio

$$Tr_A = \frac{\sigma_{\gamma^* A\to VX}}{A\sigma_{\gamma^* N\to VX}} \tag{3}$$

for the diffractive incoherent (quasielasic) production of vector mesons, $\gamma^* A \to VX$, where one sums over all final states of the target nucleus except those that contain particle (pion) creation.

If electroproduction of a vector meson leaves the target intact, the process $\gamma^* A \to VA$ is usually called coherent or elastic. For this process one can formally define the nuclear transparency in the same way, Eq. (3); however, the coherent production cross section $\sigma^{\rm coh}_{\gamma^* A\to VA}$ has a form different from the incoherent cross section $\sigma^{\rm inc}_{\gamma^* A\to VX}$, as will be seen in Secs. IV and V [see Eqs. (65) and (73)].

There are two time scales that control the dynamics of vector meson production [28]. The first time scale, called formation time, is connected with the phenomenon called color transparency. This effect comes from QCD and has been studied intensively for almost two decades. The second time scale, known as the coherence time, is connected with quantum coherence effects. Both phenomena cause nuclear suppression.

The phenomenon of CT can be treated either in the hadronic or in the quark basis. The former approach leads to Gribov's inelastic corrections [35], whereas the latter manifests itself as a result of color screening [7,8]. Although these two approaches are complementary, the quark-gluon interpretation is more intuitive and straightforward, coming from the fact that colorless hadrons can interact only because color is distributed inside them. If the hadron transverse size r tends to zero then the interaction cross section $\sigma_{\bar qq}(r)$ vanishes as r^2 [7]. As a result, the nuclear medium is more transparent for smaller transverse size hadrons. Besides, this fact naturally explains the correlation between the cross sections of hadrons and their sizes [36–38].

Diffractive electroproduction of vector mesons off nuclei is one of the most effective processes for studying CT. According to Eq. (1), in this case a photon of high virtuality $Q^2 \gg m_V^2$ is expected to produce a pair with a small transverse separation $\sim 1/Q^2$.[2] Then CT manifests itself as a vanishing absorption of the small-size colorless $\bar qq$ wave packet during propagation through the nucleus. The dynamical evolution of this small-size $\bar qq$ pair into a normal-size vector meson is controlled by the time scale called formation time. Because of the uncertainty principle, one needs a time interval to resolve different levels V (the ground state) or V' (the next excited state) in the final state. In the rest frame of the nucleus this formation time is Lorentz dilated,

$$t_f = \frac{2\nu}{m_V'^2 - m_V^2}, \tag{4}$$

where ν is the photon energy. A rigorous quantum-mechanical description of the pair evolution was suggested in Ref. [31] and is based on the nonrelativistic light-cone Green function technique. A complementary description of the same process in the hadronic basis is presented in Ref. [39].

Another phenomenon known to cause nuclear suppression is quantum coherence, which results from the destructive interference of amplitudes for which the interaction takes place on different bound nucleons. It is controlled by the distance from the production to the absorption point when the pointlike photon becomes the hadronlike $\bar qq$ pair and may be also interpreted as the lifetime of $\bar qq$ fluctuation, thus providing the time scale that controls shadowing. Again, it can be estimated by relying on the uncertainty principle and Lorentz time dilation as

$$t_c = \frac{2\nu}{Q^2 + m_V^2}. \tag{5}$$

This is usually called coherence time, but we also will use the term coherence length, since light-cone kinematics is assumed, $l_c = t_c$ (similarly, for formation length $l_f = t_f$). The CL is related to the longitudinal momentum transfer in $\gamma^* N \to VN$ as $q_c = 1/l_c$, which controls the interference of the production amplitudes from different nucleons.

Since the exclusive production of vector mesons at high energies is controlled by small-x_{Bj} physics, gluon shadowing becomes an important issue [28]. In fact, GS suppresses electroproduction of vector mesons. Although it has been shown [40] that for electroproduction of charmonia off nuclei GS starts to be important at center-of-mass energies $\sqrt{(s)} \geqslant$ 30–60 GeV, the same does not happen for electroproduction of light vector mesons [28], where GS starts to be effective at smaller energy values $\sqrt{(s)} \geqslant$ 7–30 GeV. Nevertheless, GS in the HERMES kinematical range discussed in the present paper is negligible and does not need to be included in calculations.

In electroproduction of vector mesons off nuclei one needs to disentangle CT (absorption) and CL (shadowing) as the two sources of nuclear suppression. These effects can be associated with final- and initial-state interactions, respectively. A detailed analysis of the CT and CL effects in electroproduction of vector mesons off nuclei showed [28], for a vector dominance model (VDM) example, that one can easily identify the difference of the nuclear suppression corresponding to absorption and shadowing, in the two limiting cases:

(i) The limit of l_c shorter than the mean internucleon spacing ($\sim$2 fm). In this case only final-state absorption matters. The ratio of the quasielastic (or incoherent) $\gamma^* A \to VX$ and $\gamma^* N \to VX$ cross sections, usually called nuclear

[2] In fact, the situation is somewhat more complicated. For very asymmetric pairs, when the q or $\bar q$ carry almost the whole photon momentum, the pair can have a large separation; see Sec. II.

transparency, reads [31]

$$Tr_A^{\rm inc}\Big|_{l_c\ll R_A} \equiv \frac{\sigma_V^{\gamma^* A}}{A\sigma_V^{\gamma^* N}} = \frac{1}{A}\int d^2b \int_{-\infty}^{\infty} dz\, \rho_A(b,z) \times \exp\left[-\sigma_{\rm in}^{VN}\int_z^{\infty} dz'\, \rho_A(b,z')\right] = \frac{1}{A\sigma_{\rm in}^{VN}}\int d^2b\{1-\exp\left[-\sigma_{\rm in}^{VN}T_A(b)\right]\} = \frac{\sigma_{\rm in}^{VA}}{A\sigma_{\rm in}^{VN}}. \quad (6)$$

Here z is the longitudinal coordinate and $\vec{b}$ the impact parameter of the production point of vector meson. In Eq. (6) $\rho_A(b,z)$ is the nuclear density and $\sigma_{\rm in}^{VN}$ is the inelastic VN cross section.

(ii) The limit of long l_c, where the expression for the nuclear transparency takes a different form,

$$Tr_A^{\rm inc}\Big|_{l_c\gg R_A} = \int d^2b T_A(b)\exp\left[-\sigma_{\rm in}^{VN}T_A(b)\right], \quad (7)$$

and where we assume $\sigma_{el}^{VN} \ll \sigma_{\rm in}^{VN}$ for the sake of simplicity. Here $T_A(b)$ is the nuclear thickness function

$$T_A(b) = \int_{-\infty}^{\infty} dz\, \rho_A(b,z). \quad (8)$$

The exact expression that interpolates between the two regimes (6) and (7) can be found in Ref. [41].

The problem of CT-CL separation is different depending on the mass of the produced vector meson. In the production of light vector mesons (ρ^0, Φ^0) [28] the coherence length is larger or comparable with the formation length, $l_c \gtrsim l_f$, starting from the photoproduction limit up to $Q^2 \sim 1$–2 GeV^2. For charmonium production, however, there is a strong inequality $l_c < l_f$ independent of Q^2 and ν [29,30], which therefore leads to a different scenario of CT-CL mixing.

Recently, new HERMES data [42,43] for diffractive exclusive electroproduction of ρ^0 mesons on nitrogen target have gradually become available. At the beginning the data were presented as a dependence of nuclear transparencies (3) on coherence length (5). The data for incoherent ρ^0 production decrease with l_c, as expected from the effects of initial-state interactions. In contrast, the nuclear transparency for coherent ρ^0 production increases with coherence length, as expected from the effects of the nuclear form factor [28]. However, each l_c bin of the data contains different values of ν and Q^2 (i.e., there are different contributions from both effects, CT and CL). For this reason the l_c behavior of nuclear transparency does not allow us to study CT and CL effects separately. Therefore it was proposed in Refs. [28,39] that CT can be separately studied, eliminating the effect of CL from the data on the Q^2 dependence of nuclear transparency, in a way that keeps $l_c = $ const. According to this prescription, the HERMES data [43] were later presented as the Q^2 dependence of nuclear transparency, albeit at different fixed values of l_c. Then the rise of $Tr_A^{\rm inc}$ and $Tr_A^{\rm coh}$ with Q^2 represents a signature of CT. The HERMES data [43] are in a good agreement with the predictions from Ref. [28].

New HERMES data on neon and krypton targets should be presented soon and these will allow us to verify further the predictions for CT from Ref. [28]. In addition, gradually increasing the statistics of the HERMES data should allow us to also obtain results at different polarizations L and T, and this offers the interesting possibility of studying the polarization dependence of the CT and CL effects, in both coherent and incoherent production of vector mesons. The data are usually presented as the L/T ratio R_{LT}^A of the corresponding nuclear cross sections. Knowing the nucleon L/T ratio R_{LT} one can define the nuclear modification factor as

$$f(s,Q^2,A) = \frac{R_{LT}^A}{R_{LT}} \quad (9)$$

for both coherent and incoherent processes. The nuclear modification factor represents a modification of the nucleon L/T ratio, given by a nuclear environment. Its deviation from unity allows one to obtain information about a possible different onset of CT and CL effects in the production of L and T vector mesons. Therefore an exploratory study of the Q^2 and A dependence of the factors $f_{\rm inc}$ and $f_{\rm coh}$ gives an alternative way for investigating CT and CL effects in coherent and incoherent production of vector mesons, at different polarizations L and T. This is the main goal of the present paper.

The paper is organized as follows. In Sec. II we present the light-cone approach to diffractive electroproduction of vector mesons in the rest frame of the nucleon target. Here we also describe the individual ingredients contained in the production amplitude: (i) the dipole cross section, (ii) the LC wave function for a quark-antiquark fluctuation of the virtual photon, and (iii) the LC wave function of the vector meson.

In Sec. III we calculate the nucleon L/T ratio R_{LT} of the cross sections for exclusive electroproduction of L and T polarized ρ^0, Φ^0, and charmonia. The model calculations reproduce quite well the available data for the Q^2 dependence of R_{LT}. This is an important test of the model because R_{LT} is included in the calculations of the nuclear L/T ratio.

Section IV is devoted to the incoherent production of vector mesons off nuclei. First, in Sec. IV A we define the different transparency ratios, and in Sec. IV B, we briefly describe the formalism based on the LC Green function technique. In Sec. IV C we analyze different regimes of incoherent production of vector mesons, depending on the magnitude of the coherence length. Then in Sec. IV D we present a discussion on the A and Q^2 behavior of the nuclear L/T ratio in the limit of long coherence length $l_c \gg R_A$, because in this limit the corresponding formulas and theoretical treatment get simplified with respect to the general case $l_c \sim R_A$, where there is a strong CT-CL mixing. Here we also present the model predictions for the nuclear modification factor $f_{\rm inc}$ and nuclear L/T ratio. Finally, we study the general case when there is no restriction on the coherence length. The numerical calculations of Sec. IV E produce the prediction for the L/T ratio of nuclear cross sections, for production of L and T polarized vector mesons, as a function of the mass number A at different fixed values of $\langle Q^2\rangle$ corresponding to

the HERMES kinematics. We find a monotonic A dependence of this ratio. We discuss why this A behavior of $R_{LT}^A(\text{inc})$ only weakly changes with Q^2. Following the prescription of Refs. [28,39] we also investigate how a clear signal of CT effects manifests itself separately in the production of L and T polarized vector mesons. We present the model predictions for the Q^2 dependence of f_{inc} at different fixed values of the coherence length. Such a polarization dependence of CT effects can be analyzed by the HERMES Collaboration and in the experiments at JLab.

Coherent production of vector mesons off nuclei leaving the nucleus intact is studied in Sec. V. The formalism, with an emphasis on the nuclear L/T ratio, is described in Sec. V A. Then, just as for incoherent production, we analyze in Sec. V B the A and Q^2 behavior of the nuclear L/T ratio, in the limit of long coherence length. Here we also present the corresponding model predictions for the nuclear modification factor and the L/T ratio. The general case with no restriction on the coherence length is analyzed in Sec. V C. In contrast to incoherent vector meson production, here we find, at medium and large values of Q^2 (when $l_c \lesssim R_A$, where R_A is the nuclear radius), a nonmonotonic A dependence of the nuclear L/T ratio. This nontrivial and anomalous A dependence of $R_{LT}^A(\text{coh})$ is even more complicated at larger values of Q^2, as a result of a stronger interplay between CT and CL effects. We find also a different manifestation of the net CT effects in the production of L and T polarized vector mesons, by performing the predictions at fixed values of the coherence length.

Gluon shadowing starts to manifest itself at $\sqrt{s} \geqslant$ 7–30 GeV and is not significant in the HERMES energy range studied in the present paper. Therefore it is not included in the calculations.

The results of the paper are summarized and discussed in Sec. VI. The important conclusion of a nontrivial A dependence of the coherent nuclear L/T ratio for the expected new HERMES data and for the future planned experiments is stressed.

II. COLOR DIPOLE PHENOMENOLOGY FOR ELASTIC ELECTROPRODUCTION OF VECTOR MESONS $\gamma^* N \to V N$

The LC dipole approach for elastic electroproduction $\gamma^* N \to V N$ was already used in Ref. [44] to study the exclusive photo- and electroproduction of charmonia, and in Ref. [28] for elastic virtual photoproduction of the light vector mesons ρ^0 and Φ^0 (for a review see also Ref. [45]). Therefore, we present only a short review of this LC phenomenology, with the main emphasis on looking at the effects of the different polarizations L and T. In this approach a diffractive process is treated as elastic scattering of a $\bar{q}q$ fluctuation of the incident particle. The elastic amplitude is given by convolution of the universal flavor-independent dipole cross section for the $\bar{q}q$ interaction with a nucleon, $\sigma_{\bar{q}q}$ [7], and the initial and final wave functions. For the exclusive photo- or electroproduction of vector mesons $\gamma^* N \to V N$ the forward production amplitude is represented in the following form:

$$\begin{aligned}\mathcal{M}_{\gamma^* N \to V N}(s, Q^2) &= \langle V | \sigma_{\bar{q}q}(\vec{r}, s) | \gamma^* \rangle \\ &= \int_0^1 d\alpha \int d^2 r \Psi_V^*(\vec{r}, \alpha) \sigma_{\bar{q}q}(\vec{r}, s) \\ &\quad \times \Psi_{\gamma^*}(\vec{r}, \alpha, Q^2), \end{aligned} \tag{10}$$

with the normalization

$$\left.\frac{d\sigma(\gamma^* N \to V N)}{dt}\right|_{t=0} = \frac{|\mathcal{M}_{\gamma^* N \to V N}(s, Q^2)|^2}{16\pi}. \tag{11}$$

There are three ingredients contributing to the amplitude (10):

(i) the dipole cross section $\sigma_{\bar{q}q}(\vec{r}, s)$, which depends on the $\bar{q}q$ transverse separation $\vec{r}$ and the c.m. energy squared s,
(ii) the LC wave function of the photon $\Psi_{\gamma^*}(\vec{r}, \alpha, Q^2)$, which depends also on the photon virtuality Q^2 and the relative share α of the photon momentum carried by the quark, and
(iii) the LC wave function $\Psi_V(\vec{r}, \alpha)$ of the vector meson.

Notice that in the LC formalism the photon and meson wave functions also contain higher Fock states $|\bar{q}q\rangle$, $|\bar{q}qG\rangle$, $|\bar{q}q2G\rangle$, etc. The effects of higher Fock states are implicitly incorporated into the energy dependence of the dipole cross section $\sigma_{\bar{q}q}(\vec{r}, s)$, as is given in Eq. (10).

A. Dipole cross section

The dipole cross section $\sigma_{\bar{q}q}(\vec{r}, s)$ represents the interaction of a $\bar{q}q$ dipole of transverse separation $\vec{r}$ with a nucleon [7]. It is a flavor-independent universal function of $\vec{r}$ and energy, and allows us to describe in a uniform way various high-energy processes. It is known to vanish quadratically [$\sigma_{\bar{q}q}(r, s) \propto r^2$] as $r \to 0$, owing to color screening (CT property). The dipole cross section cannot be predicted reliably because of poorly known higher order pQCD corrections and nonperturbative effects. A detailed discussion of the dipole cross section in connection with production of vector mesons is presented in Ref. [28].

There are two popular parametrizations of $\sigma_{\bar{q}q}(\vec{r}, s)$. The first, suggested in Ref. [46], reflects the fact that at small separations the dipole cross section should be a function of r and $x_{Bj} \sim 1/(r^2 s)$, to reproduce Bjorken scaling. It describes well data for deep-inelastic scattering (DIS) at small x_{Bj} and medium and high Q^2. However, at small Q^2 it cannot be correct since it predicts energy-independent hadronic cross sections. Besides, x_{Bj} is no longer a proper variable at small Q^2 and should be replaced by energy. This defect is removed by the second parametrization proposed in Ref. [27], which is similar to the first one [46] but contains an explicit dependence on energy, and it is valid down to the limit of real photoproduction. Since we will consider HERMES data with a typical kinematical region of the photon energy, $5 < \nu < 24$ GeV, and virtuality, $0.8 < Q^2 < 5$ GeV^2, we choose the second parametrization, which has the following form:

$$\sigma_{\bar{q}q}(r, s) = \sigma_0(s)\left[1 - e^{-r^2/r_0^2(s)}\right], \tag{12}$$

where

$$\sigma_0(s) = \sigma_{\rm tot}^{\pi p}(s)\left[1 + \frac{3}{8}\frac{r_0^2(s)}{\langle r_{\rm ch}^2\rangle}\right] \text{ mb} \tag{13}$$

and

$$r_0(s) = 0.88\left(\frac{s}{s_0}\right)^{-0.14} \text{ fm}. \tag{14}$$

Here $\langle r_{\rm ch}^2\rangle = 0.44$ fm^2 is the mean pion charge radius squared, and $s_0 = 1000$ GeV^2. The cross section $\sigma_{\rm tot}^{\pi p}(s)$ was fitted to data in Ref. [47,48] and reads

$$\sigma_{\rm tot}^{\pi p}(s) = 23.6\left(\frac{s}{s_0}\right)^{0.079} + 1.425\left(\frac{s}{s_0}\right)^{-0.45} \text{ mb}. \tag{15}$$

This represents the Pomeron and Reggeon parts, corresponding to exchange of gluons and $\bar{q}q$, respectively. A detailed description of the incorporation of Reggeons into the LC dipole formalism can be found in Ref. [28].

The dipole cross section presented in Eqs. (12)–(15) provides the imaginary part of the elastic amplitude. It is known, however, that the energy dependence of the total cross section also generates a real part [49],

$$\sigma_{\bar{q}q}(r,s) \Rightarrow \left(1 - i\frac{\pi}{2}\frac{\partial}{\partial \ln(s)}\right)\sigma_{\bar{q}q}(r,s). \tag{16}$$

Therefore the energy dependence of the dipole cross section given by Eq. (12), which is rather steep at small r, leads to a large real part that should not be neglected.

B. The $\bar{q}q$ wave function of the photon

The perturbative distribution amplitude ("wave function") of the $\bar{q}q$ Fock component of the photon has the following form, for T and L polarized photons [50–52]:

$$\Psi_{\bar{q}q}^{T,L}(\vec{r},\alpha) = \frac{\sqrt{N_C\alpha_{\rm em}}}{2\pi} Z_q \bar{\chi}\hat{O}^{T,L}\chi K_0(\epsilon r), \tag{17}$$

where χ and $\bar{\chi}$ are the spinors of the quark and antiquark, respectively, Z_q is the quark charge, with $Z_q = 1/\sqrt{2}, 1/3\sqrt{2}, 1/3, 2/3,$ and $1/3$ for $\rho^0, \omega^0, \Phi^0, J/\Psi$, and Υ production respectively, $N_C = 3$ is the number of colors. and $K_0(\epsilon r)$ is a modified Bessel function with

$$\epsilon^2 = \alpha(1-\alpha)Q^2 + m_q^2. \tag{18}$$

Here m_q is the quark mass, and α is the fraction of the LC momentum of the photon carried by the quark. The operators $\widehat{O}^{T,L}$ are given by

$$\widehat{O}^T = m_q\vec{\sigma}\cdot\vec{e} + i(1-2\alpha)(\vec{\sigma}\cdot\vec{n})(\vec{e}\cdot\vec{\nabla}_r) + (\vec{\sigma}\times\vec{e})\cdot\vec{\nabla}_r, \tag{19}$$

$$\widehat{O}^L = 2Q\alpha(1-\alpha)(\vec{\sigma}\cdot\vec{n}). \tag{20}$$

Here $\vec{\nabla}_r$ acts on the transverse coordinate $\vec{r}$, $\vec{e}$ is the polarization vector of the photon, $\vec{n}$ is a unit vector parallel to the photon momentum, and $\vec{\sigma}$ is the three-vector of the Pauli spin matrices.

The transverse separation of the $\bar{q}q$ pair contains an explicit α dependence and can be written uby sing the expression for the scanning radius, Eq. (1), as

$$r_{\bar{q}q} \sim \frac{1}{\epsilon} = \frac{1}{\sqrt{Q^2\alpha(1-\alpha)+m_q^2}} \sim \frac{r_S}{3} = \frac{\tilde{Y}}{\sqrt{Q^2+m_V^2}}, \tag{21}$$

where $\tilde{Y} = Y/3$. For very asymmetric $\bar{q}q$ pairs the LC variable α or $(1-\alpha) \lesssim m_q^2/Q^2$. Consequently, the transverse separation $r_{\bar{q}q} \sim \tilde{1}/m_q$ and the scanning radius r_S become large. However, this is not the case of charmonium and bottonium production because of the large quark masses $m_c = 1.5$ GeV and $m_b = 5.0$ GeV, respectively. Therefore in this latter case it is straightforward to include nonperturbative interaction effects between q and $\bar{q}$. In the production of light vector mesons there are two ways to fix the problem of a huge $\bar{q}q$ transverse separation. One can introduce an effective quark mass $m_q \approx \Lambda_{\rm QCD}$, which should represent the nonperturbative interaction effects between the q and $\bar{q}$, or one can introduce this interaction explicitly. We use the second possibility, with the corresponding phenomenology based on the LC Green function approach developed in Ref. [27].

The Green function $G_{\bar{q}q}(z_1,\vec{r}_1;z_2,\vec{r}_2)$ describes the propagation of an interacting $\bar{q}q$ pair between points with longitudinal coordinates z_1 and z_2, and with initial and final separations $\vec{r}_1$ and $\vec{r}_2$. This Green function satisfies the two-dimensional Schrödinger equation,

$$i\frac{d}{dz_2}G_{\bar{q}q}(z_1,\vec{r}_1;z_2,\vec{r}_2) = \left\{\frac{\epsilon^2-\Delta_{r_2}}{2\nu\alpha(1-\alpha)} + V_{\bar{q}q}(z_2,\vec{r}_2,\alpha)\right\}G_{\bar{q}q}(z_1,\vec{r}_1;z_2,\vec{r}_2). \tag{22}$$

Here ν is the photon energy, and the Laplacian Δ_r acts on the coordinate r.

The imaginary part of the LC potential $V_{\bar{q}q}(z_2,\vec{r}_2,\alpha)$ in Eq. (22) is responsible for the attenuation of the $\bar{q}q$ in the medium, whereas the real part represents the interaction between the q and $\bar{q}$. This potential is supposed to provide the correct LC wave functions of the vector mesons. For the sake of simplicity we use the oscillator form of the potential,

$$\text{Re}V_{\bar{q}q}(z_2,\vec{r}_2,\alpha) = \frac{a^4(\alpha)\vec{r}_2^2}{2\nu\alpha(1-\alpha)}, \tag{23}$$

which leads to a Gaussian r dependence of the LC wave function of the meson ground state. The shape of the function $a(\alpha)$ will be discussed in the following.

In this case Eq. (22) has an analytical solution, leading to an explicit form of the harmonic oscillator Green function [53],

$$G_{\bar{q}q}(z_1,\vec{r}_1;z_2,\vec{r}_2) = \frac{a^2(\alpha)}{2\pi i\sin(\omega\Delta z)}\exp\left\{\frac{ia^2(\alpha)}{\sin(\omega\Delta z)}\left[\left(r_1^2+r_2^2\right)\cos(\omega\Delta z) - 2\vec{r}_1\cdot\vec{r}_2\right]\right\}\exp\left[-\frac{i\epsilon^2\Delta z}{2\nu\alpha(1-\alpha)}\right], \tag{24}$$

where $\Delta z = z_2 - z_1$ and

$$\omega = \frac{a^2(\alpha)}{\nu\alpha(1-\alpha)}. \tag{25}$$

The boundary condition is $G_{\bar{q}q}(z_1, \vec{r}_1; z_2, \vec{r}_2)|_{z_2=z_1} = \delta^2(\vec{r}_1 - \vec{r}_2)$.

The probability amplitude of finding the $\bar{q}q$ fluctuation of a photon at the point z_2 with separation $\vec{r}$ is given by an integral over the point z_1 where the $\bar{q}q$ is created by the photon with initial separation zero:

$$\Psi^{T,L}_{\bar{q}q}(\vec{r}, \alpha) = \frac{iZ_q\sqrt{\alpha_{\rm em}}}{4\pi\nu\alpha(1-\alpha)} \times \int_{-\infty}^{z_2} dz_1 \, (\bar{\chi}\widehat{O}^{T,L}\chi) G_{\bar{q}q}(z_1, \vec{r}_1; z_2, \vec{r})\Big|_{r_1=0}. \tag{26}$$

The operators $\widehat{O}^{T,L}$ are defined by Eqs. (19) and (20). Here they act on the coordinate $\vec{r}_1$.

If we write the transverse part as

$$\bar{\chi}\widehat{O}^T\chi = \bar{\chi}m_q\vec{\sigma}\cdot\vec{e}\chi + \bar{\chi}[i(1-2\alpha)(\vec{\sigma}\cdot\vec{n})\vec{e} + (\vec{\sigma}\times\vec{e})]\chi\cdot\vec{\nabla}_r = E + \vec{F}\cdot\vec{\nabla}_r, \tag{27}$$

then the distribution functions read

$$\Psi^T_{\bar{q}q}(\vec{r}, \alpha) = Z_q\sqrt{\alpha_{\rm em}}[E\Phi_0(\epsilon, r, \lambda) + \vec{F}\cdot\vec{\Phi}_1(\epsilon, r, \lambda)], \tag{28}$$

$$\Psi^L_{\bar{q}q}(\vec{r}, \alpha) = 2Z_q\sqrt{\alpha_{\rm em}}Q\alpha(1-\alpha)\bar{\chi}\vec{\sigma}\cdot\vec{n}\chi\,\Phi_0(\epsilon, r, \lambda), \tag{29}$$

where

$$\lambda = \frac{2a^2(\alpha)}{\epsilon^2}. \tag{30}$$

The functions $\Phi_{0,1}$ in Eqs. (28) and (29) are defined as

$$\Phi_0(\epsilon, r, \lambda) = \frac{1}{4\pi}\int_0^\infty dt \frac{\lambda}{{\rm sh}(\lambda t)} \times \exp\left[-\frac{\lambda\epsilon^2 r^2}{4}\,{\rm cth}(\lambda t) - t\right], \tag{31}$$

$$\vec{\Phi}_1(\epsilon, r, \lambda) = \frac{\epsilon^2\vec{r}}{8\pi}\int_0^\infty dt \left[\frac{\lambda}{{\rm sh}(\lambda t)}\right]^2 \times \exp\left[-\frac{\lambda\epsilon^2 r^2}{4}{\rm cth}(\lambda t) - t\right], \tag{32}$$

where ${\rm sh}(x)$ and ${\rm cth}(x)$ are the hyperbolic sine and hyperbolic cotangent, respectively. Note that the $\bar{q}$-q interaction enters Eqs. (28) and (29) via the parameter λ defined in Eq. (30). In the limit of vanishing interaction ($\lambda \to 0$; i.e., $Q^2 \to \infty, \alpha$ fixed, $\alpha \neq 0$ or 1), Eqs. (28) and (29) produce the perturbative expressions of Eq. (17). As previously mentioned, for charmonium and bottonium production nonperturbative interaction effects are weak. Consequently, the parameter λ is then rather small owing to the large quark masses $m_c = 1.5$ GeV and $m_b = 5.0$ GeV, and it is given by

$$\lambda = \frac{8a^2(\alpha)}{Q^2 + 4m^2_{c,b}}. \tag{33}$$

With the choice $a^2(\alpha) \propto \alpha(1-\alpha)$ the end-point behavior of the mean-square interquark separation $\langle r^2\rangle \propto 1/\alpha(1-\alpha)$ contradicts the idea of confinement. Following Ref. [27] we fix this problem via a simple modification of the LC potential,

$$a^2(\alpha) = a_0^2 + 4a_1^2\alpha(1-\alpha). \tag{34}$$

The parameters a_0 and a_1 were adjusted in Ref. [27] to data on total photoabsorption cross section [54,55], diffractive photon dissociation, and shadowing in nuclear photoabsorption reactions. The results of our calculations vary within only 1% when a_0 and a_1 satisfy the relations

$$a_0^2 = v^{1.15}(0.112)^2\ {\rm GeV}^2, \qquad a_1^2 = (1-v)^{1.15}(0.165)^2\ {\rm GeV}^2, \tag{35}$$

where v takes any value in the range $0 < v < 1$. In view of this insensitivity of the observables we fix the parameters at $v = 1/2$. We checked that this choice does not affect our results beyond a few percent uncertainty.

C. Vector meson wave function

The last ingredient in the elastic production amplitude (10) is the vector meson wave function. We use the popular prescription of Ref. [56], obtained by applying a Lorentz boost to the rest-frame wave function, assumed to be Gaussian, which in turn leads to radial parts of transversely and longitudinally polarized mesons in the form (for an alternative description of the vector meson wave function see Refs. [57,58])

$$\Phi^{T,L}_V(\vec{r}, \alpha) = C^{T,L}\alpha(1-\alpha)f(\alpha)\exp\left[-\frac{\alpha(1-\alpha)\vec{r}^2}{2R^2}\right], \tag{36}$$

with the normalization defined in the following, and

$$f(\alpha) = \exp\left[-\frac{m_q^2R^2}{2\alpha(1-\alpha)}\right], \tag{37}$$

with the parameters, taken from Ref. [24], $R = 0.515$ fm, $m_q = 0.1$ GeV for ρ^0 production; $R = 0.415$ fm, $m_q = 0.3$ GeV for Φ^0 production; $R = 0.183$ fm, $m_q = 1.3$ GeV for charmonium production; and $R = 0.061$ fm, $m_q = 5.0$ GeV for bottonium production.

We assume that the distribution amplitude of the $\bar{q}q$ fluctuations for both the vector meson and the photon have a similar structure [24]. Then in analogy to Eqs. (28) and (29),

$$\Psi^T_V(\vec{r}, \alpha) = (E + \vec{F}\cdot\vec{\nabla}_r)\Phi^T_V(\vec{r}, \alpha), \tag{38}$$

$$\Psi^L_V(\vec{r}, \alpha) = 2m_V\alpha(1-\alpha)(\bar{\chi}\vec{\sigma}\cdot\vec{n}\chi)\Phi^L_V(\vec{r}, \alpha). \tag{39}$$

Correspondingly, the normalization conditions for the transverse and longitudinal vector meson wave functions read

$$N_C \int d^2r \int d\alpha \Big[m_q^2 \big|\Phi_V^T(\vec{r},\alpha)\big|^2 + [\alpha^2 + (1-\alpha)^2] \big|\partial_r \Phi_V^T(\vec{r},\alpha)\big|^2 \Big] = 1 \qquad (40)$$

and

$$4N_C \int d^2r \int d\alpha \alpha^2 (1-\alpha)^2 m_V^2 \big|\Phi_V^L(\vec{r},\alpha)\big|^2 = 1. \qquad (41)$$

III. ELECTROPRODUCTION OF VECTOR MESONS ON A NUCLEON: COMPARISON WITH DATA

As the first test of the formalism, in this section we verify the LC approach by comparing its results with data for nucleon targets. Since the expected new HERMES data will be, at separate polarizations L and T, predominantly for electroproduction of ρ^0, we focus our attention on the production of light vector mesons. Using all the ingredients specified in the previous section [i.e., the nonperturbative photon equations (28) and (29) and vector meson wave function equations (38) and (39)], we can calculate the forward production amplitude $\gamma^* N \to VN$ for transverse and longitudinal photons and vector mesons. Under the assumption of s-channel helicity conservation (SCHC), the forward scattering amplitude reads

$$\mathcal{M}^T_{\gamma^* N \to VN}(s,Q^2)\big|_{t=0} = N_C Z_q \sqrt{2\alpha_{\rm em}} \int d^2r \sigma_{\bar{q}q}(\vec{r},s) \times \int_0^1 d\alpha \big\{ m_q^2 \Phi_0(\epsilon,\vec{r},\lambda)\Phi_V^T(\vec{r},\alpha) - [\alpha^2 + (1-\alpha)^2]\vec{\Phi}_1(\epsilon,\vec{r},\lambda) \times \vec{\nabla}_r \Phi_V^T(\vec{r},\alpha)\big\}, \qquad (42)$$

$$\mathcal{M}^L_{\gamma^* N \to VN}(s,Q^2)\big|_{t=0} = 4N_C Z_q \sqrt{2\alpha_{\rm em}} m_V Q \int d^2r \sigma_{\bar{q}q}(\vec{r},s) \times \int_0^1 d\alpha \alpha^2 (1-\alpha)^2 \times \Phi_0(\epsilon,\vec{r},\lambda)\Phi_V^L(\vec{r},\alpha). \qquad (43)$$

These amplitudes are normalized as $|\mathcal{M}^{T,L}|^2 = 16\pi d\sigma_N^{T,L}/dt|_{t=0}$, and their real parts are included according to the prescription described in Sec. II. The terms $\propto \Phi_0(\epsilon,\vec{r},\lambda)\Phi_V(\vec{r},\alpha)$ and $\propto \vec{\Phi}_1(\epsilon,\vec{r},\lambda)\cdot\vec{\nabla}_r\Phi_V(\vec{r},\alpha)$ in Eqs. (42) and (43) correspond to the helicity-conserving and helicity-flip transitions in the $\gamma^* \to \bar{q}q, V \to \bar{q}q$ vertices, respectively. The helicity-flip transitions represent the relativistic corrections. For heavy quarkonium these corrections become important only at large $Q^2 \gg m_V^2$. For production of light vector mesons, however, they are non-negligible even in the photoproduction limit, $Q^2 = 0$.

Usually the data are presented in the form of the production cross section $\sigma = \sigma^T + \epsilon'\sigma^L$, at fixed photon polarization ϵ'. Here the cross section integrated over t reads

$$\sigma^{T,L}(\gamma^* N \to VN) = \frac{|\mathcal{M}^{T,L}|^2}{16\pi B_{\gamma^* N}}, \qquad (44)$$

where $B_{\gamma^* N} \equiv B$ is the slope parameter in the reaction $\gamma^* p \to Vp$. The absolute value of the production cross section has already been checked by comparing with data for elastic ρ^0 and Φ^0 electroproduction in Ref. [28] and for charmonium exclusive electroproduction $\gamma^* p \to J/\Psi p$ in Refs. [29,30].

Motivated by the expected data from the HERMES Collaboration, we are going to make predictions for the production cross sections $\sigma^{L,T}(\gamma^* N \to VN)$ at separate polarizations L and T. However, the data are usually presented as the ratio $R_{LT} = \sigma_L(\gamma^* N \to VN)/\sigma_T(\gamma^* N \to VN)$ at different photon virtualities Q^2. Then a deviation of R_{LT} from unity indicates a difference in the production mechanisms of L and T polarized vector mesons. To calculate the ratio R_{LT}, using Eqs. (42) and (43) for forward production amplitudes at different polarizations L and T, one should know corresponding slope parameters $B_{\gamma_L^* N} \equiv B_L$ and $B_{\gamma_T^* N} \equiv B_T$:

$$R_{LT} = \frac{|\mathcal{M}^L|^2}{|\mathcal{M}^T|^2}\frac{B_T}{B_L} \approx \frac{|\mathcal{M}^L|^2}{|\mathcal{M}^T|^2}\left(1 + \frac{\Delta B_{TL}}{B}\right), \qquad (45)$$

where $\Delta B_{TL} = B_T - B_L$.

The scanning phenomenon, Eq. (1), was already discussed in Refs. [22,24,59], and it can be understood qualitatively by analyzing the forward production amplitude (10). Here we assume for simplicity the perturbative distribution amplitudes of the $\bar{q}q$ Fock component of the photon containing the Bessel function $K_0(\epsilon r)$ [see Eq. (17)]. As was mentioned in the previous section, the most important property of the dipole cross section $\sigma_{\bar{q}q}(\vec{r},s)$ is the CT-driven dependence $\propto r^2$ at small r. Because of the smooth shape of the vector meson wave functions $\Phi_V^{L,T}(r,\alpha)$ [see Eq. (36)] and because of the behavior of the Bessel functions $K_{0,1}(x) \propto \exp(-x)$ at large values of x, the production amplitude is dominated by the contribution from $r_S \approx 3/\epsilon$. In the nonrelativistic approximation of $m_V \sim 2m_q$ and $\alpha \sim 0.5$, it leads to the scanning radius [Eq. (1)] and the estimate $Y \approx 6$ (see also Fig. 1). In general, to be more precise, the scanning property [see Eq. (1)] is quantified separately for L and T polarizations via the Q^2-dependent scale parameters Y_L and Y_T, as illustrated in Fig. 1. The dotted line represents the fact that for electroproduction of bottonia both scale parameters $Y_T \sim Y_L \sim 6$, and they practically do not depend on Q^2 as a consequence of the nonrelativistic approximation. Dashed lines describe the Q^2 dependence of Y_L and Y_T for charmonium electroproduction. One can see that both Y_L and Y_T smoothly rise with Q^2, do not differ much from each other, and are a little bit higher than the value 6 resulting from the nonrelativistic approximation. For this reason charmonium can be safely treated as a nonrelativistic object at small and medium values of Q^2 such that $r_S \gtrsim R_{J/\Psi}$.[3] At larger $Q^2 \gg m_{J/\Psi}^2$, the scale parameters $Y_{L,T}$ have a stronger Q^2 dependence, reaching $\sim$7.7 at $Q^2 = 100$ GeV^2, which differs from the nonrelativistic value $Y \sim 6$. This means that relativistic effects are no longer negligible and should be included in the calculations [59]. However, the situation is completely different for light vector meson production, as illustrated in Fig. 1 by the solid lines. In this case, the presence

[3] $R_{J/\Psi}$ is the radius of charmonium.

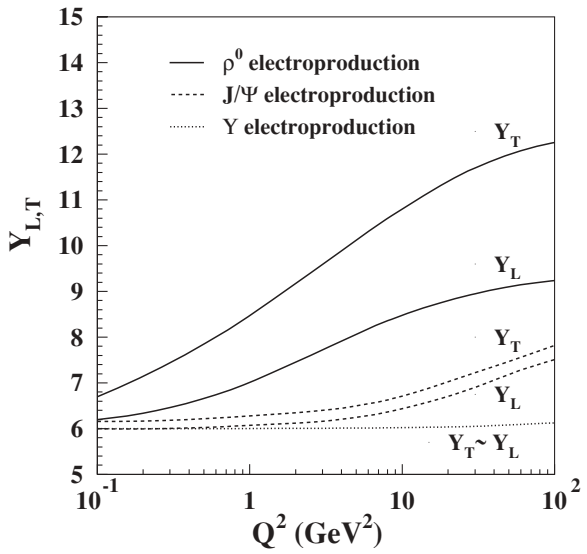

FIG. 1. Q^2 dependence of the scale parameters Y_L and Y_T, from the expression for the scanning radius [Eq. (1)], corresponding to the production of L and T polarized vector mesons. Solid, dashed, and dotted lines represent electroproduction of ρ^0, J/Ψ, and Υ, respectively.

of strong relativistic effects causes the scale parameters to rise with Q^2 much more rapidly than for the production of heavy vector mesons.

Compared to $\mathcal{M}_L$ [Eq. (42)] the transverse production amplitude $\mathcal{M}_T$ [Eq. (43)] receives larger contributions from large-size asymmetric end-point $\bar{q}q$ fluctuations with $\alpha(1-\alpha) \ll 1$. This is illustrated in Fig. 1, where $Y_T > Y_L$ in the whole Q^2 range, and the difference between Y_T and Y_L rises with Q^2. This fact is especially evident for the electroproduction of ρ^0 mesons, depicted by the solid lines. For electroproduction of charmonia the difference between Y_T and Y_L is small as a consequence of small relativistic effects, whereas for electroproduction of bottonia it was already indicated in Ref. [59] that $Y_T \sim Y_L \sim 6$ in a very broad Q^2 range, which supports the conclusion that the relativistic corrections are negligible.

At small $r_S \lesssim R_V$, the production amplitudes (42) and (43) can be evaluated as

$$\mathcal{M}_T \propto r_S^2 \sigma_{\bar{q}q}(r_S, s) \propto \frac{Y_T^4}{\left(Q^2 + m_V^2\right)^2}, \tag{46}$$

$$\mathcal{M}_L \propto \frac{\sqrt{Q^2}}{m_V} r_S^2 \sigma_{\bar{q}q}(r_S, s) \propto \frac{\sqrt{Q^2}}{m_V} \frac{Y_L^4}{\left(Q^2 + m_V^2\right)^2} \propto \frac{\sqrt{Q^2}}{m_V} \frac{Y_L^4}{Y_T^4} \mathcal{M}_T, \tag{47}$$

which means that the longitudinally polarized vector mesons dominate at $Q^2 \gg m_V^2$.

A detailed analysis of the diffraction cone [59,60] for exclusive vector meson electroproduction, within the color dipole generalized Balitskij-Fadin-Kuraev-Lipatov (BFKL) phenomenology, showed the presence of geometrical contributions from the target nucleon $\sim B_N$ and the beam dipole $\sim r^2$. At fixed energy and according to the scanning phenomenon [Eq. (1)], the diffraction slope is predicted to decrease with $(Q^2 + m_V^2)$ as

$$B(Q^2) \sim B_N + \tilde{C} r_S^2 \approx B_N + \text{const} \frac{Y^2}{Q^2 + m_V^2}. \tag{48}$$

One can see from Eq. (48) that different scanning properties for L and T polarized vector mesons ($Y_L < Y_T$; see Fig. 1 and subsequent discussion) lead also to an inequality $B_L < B_T$ of the slope parameters in the reactions $\gamma_L^* N \to V_L N$ and $\gamma_T^* N \to V_T N$. Consequently, the difference ΔB_{TL} in Eq. (45) is positive and can be estimated as

$$\Delta B_{TL} \propto \frac{\Delta Y_{TL}^2}{Q^2 + m_V^2}, \tag{49}$$

where

$$\Delta Y_{TL}^2 = Y_T^2 - Y_L^2. \tag{50}$$

For electroproduction of ρ^0 mesons at small $Q^2 \lesssim m_\rho^2$ the rise of ΔY_{TL}^2 with Q^2 can compensate or even overcompensate the decrease of ΔB_{TL} with $(Q^2 + m_\rho^2)$. Consequently, the difference ΔB_{TL} in Eq. (49) can weakly rise with Q^2. This does not happen at larger $Q^2 > m_\rho^2$, when ΔB_{TL} decreases slowly with Q^2. In the HERMES kinematical range $\Delta B_{TL} \sim 0.7\,\text{GeV}^{-2}$ at $Q^2 = 0.7\,\text{GeV}^2$, reaching a value of $\sim 0.4\,\text{GeV}^{-2}$ at $Q^2 = 5\ \text{GeV}^2$. Correspondingly, the factor $\Delta B_{TL}/B$ in Eq. (45), treated as a correction to unity in the brackets, is about 0.09 at $Q^2 = 0.7\ \text{GeV}^2$ and decreases very slowly with Q^2, reaching a value of ~ 0.07 at $Q^2 = 5\,\text{GeV}^2$. For this reason the factor $\Delta B_{TL}/B$ cannot be neglected in the calculations.

Using Eqs. (45) and (47) one can present the nucleon L/T ratio as

$$R_{LT} \propto \frac{Q^2}{m_V^2} \frac{Y_L^8}{Y_T^8} \frac{B_T}{B_L} \approx \frac{Q^2}{m_V^2} F_Y(Q^2) \left(1 + \frac{\Delta B_{TL}}{B}\right), \tag{51}$$

and thus R_{LT} is given mainly by three ingredients:

(i) The factor Q^2/m_V^2, which comes from σ_L [see Eq. (43)], represents a generic consequence of electromagnetic gauge invariance.

(ii) The Q^2-dependent factor $F_Y(Q^2) = Y_L^8/Y_T^8$, which comes from the scanning phenomenon [Eq. (1)], reflects the different relativistic corrections for the L and T production amplitudes. These corrections become important only at large $Q^2 \gg m_V^2$ (see Fig. 1). The factor F_Y leads to a substantial reduction of the rise of R_{LT} with Q^2, especially for the production of light vector mesons.

(iii) The factor B_T/B_L follows from the fact that the slope parameters B_L and B_T for the production of L and T polarized vector mesons are different. According to the scanning property ($B_L < B_T$), this factor decreases slightly with Q^2, tending to unity from above at large $Q^2 \gg m_V^2$ [59]. The ratio B_T/B_L leads to an additional but small reduction of the Q^2 rise of R_{LT}.

Our predictions are plotted in Figs. 2 and 3, together with the data on the Q^2 dependence of the ratio R_{LT} for the production of ρ^0 and Φ^0 mesons, taken from Ref. [21]. We added also the

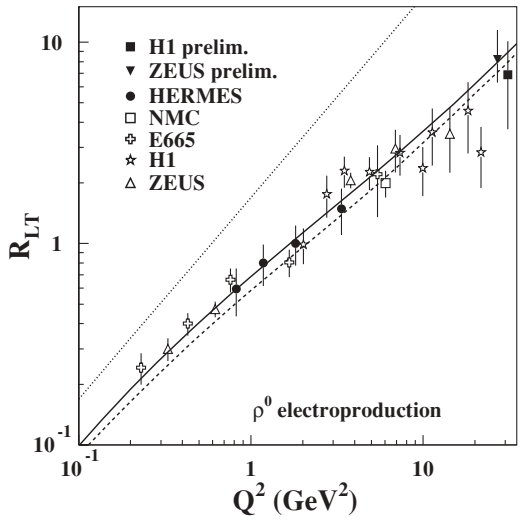

FIG. 2. Q^2 dependence of the ratio R_{LT} of the integrated cross sections for the reactions $\gamma_L^* p \to \rho_L^0 p$ and $\gamma_T^* p \to \rho_T^0 p$. The solid and dashed lines represent model calculations at $W = 15$ and 90 GeV, respectively. The data are taken from Ref. [21]. The preliminary H1 and ZEUS data can be found in Refs. [18] and [14], respectively. The dotted curve represents the Q^2/m_V^2 rise of R_{LT}.

last published data from H1 [16] and preliminary data from the H1 [18] and ZEUS [14,15] Collaborations. The analogous Q^2 dependence of R_{LT} for electroproduction of charmonia is plotted in Fig. 4 together with results from the H1 [61] and ZEUS [62] Collaborations.

One can see from Eq. (51) that the Q^2 rise of the nucleon ratio R_{LT} gets diminished by the factor F_Y, coming from the different scanning properties of the L and T production amplitudes, and by the ratio of the slope parameters B_T

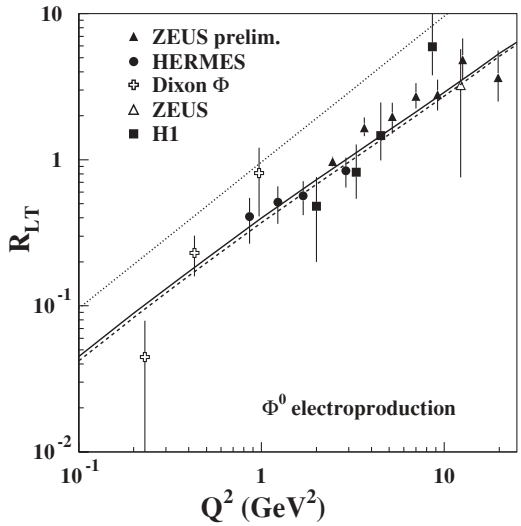

FIG. 3. Q^2 dependence of the ratio R_{LT} of the integrated cross sections for the reactions $\gamma_L^* p \to \Phi_L^0 p$ and $\gamma_T^* p \to \Phi_T^0 p$. The solid and dashed lines represent model calculations at $W = 15$ and 90 GeV, respectively. The data are taken from Ref. [21] and H1 data are from Ref. [16]. The preliminary ZEUS data can be found in Ref. [15]. The dotted curve represents the Q^2/m_V^2 rise of R_{LT}.

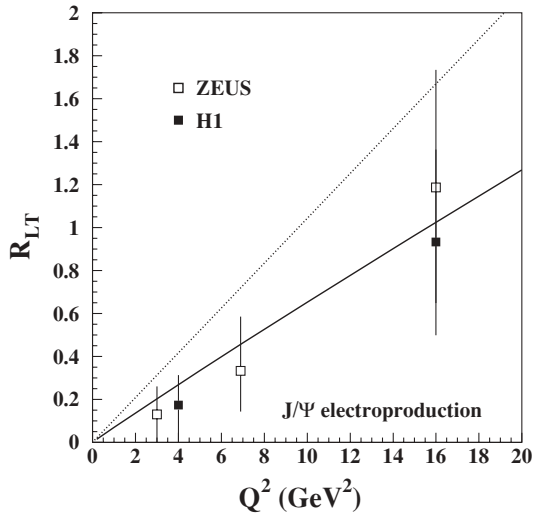

FIG. 4. Q^2 dependence of the ratio R_{LT} of the integrated cross sections for the reactions $\gamma_L^* p \to (J/\Psi)_L p$ and $\gamma_T^* p \to (J/\Psi)_T p$. The model calculations are performed at $W = 90$ GeV. The H1 and ZEUS data are taken from Refs. [61] and [62], respectively. The dotted curve represents the Q^2/m_V^2 rise of R_{LT}.

and B_L. In the nonrelativistic approximation, represented by the electroproduction of bottonia, the factor $F_Y \sim 1$ [see Eq. (51) and Fig. 1] and $B_T \sim B_L$. Consequently, the ratio R_{LT} rises with Q^2 as $\sim Q^2/m_V^2$ [59]. However, electroproduction of light vector mesons has large relativistic effects and the different scanning properties for the L and T production amplitudes ($Y_L < Y_T$) lead to a large decrease of the dominance of the longitudinal cross section $\propto |\mathcal{M}_L|^2$. Thus the ratio R_{LT} rises with Q^2 much less rapidly than Q^2/m_V^2. This is illustrated in Figs. 2 and 3 as a difference between the solid (dashed) and dotted lines. For charmonium production the decrease of the rise of the ratio R_{LT} with $Q^2/m_{J/\Psi}^2$ is much less effective because of smaller relativistic effects, as one can see in Fig. 4 as a difference between the solid and dotted lines. Notice that in all calculations we assumed SCHC as the consequence of the spin independence of the dipole cross section $\sigma_{\bar{q}q}(r, s)$ in the forward production amplitude [Eq. (10)]. This assumption is supported by the low-energy data, indicating that the amplitude for the photon-vector meson transition is predominantly s-channel conserving (i.e., the helicity of the vector meson is equal to that of the photon when the spin-quantization axis is chosen along the direction of the meson momentum in the $\gamma^* p$ center-of-mass system). In general, however, small helicity-single-flip and helicity-double-flip contributions to the production amplitude have been reported in $\pi^+\pi^-$ photoproduction in the ρ^0 mass region, at $W \lesssim 4$ GeV [63]. Helicity-single-flip amplitudes have also been observed in ρ^0 electroproduction for $1.3 < W < 2.8$ GeV and $0.3 < Q^2 < 1.4$ GeV^2 [64]. A helicity-single-flip contribution of $(14 \pm 8)\%$ was measured in ρ^0 muo production at $W = 17$ GeV [3].

At high energy the breaking of SCHC has been measured by the ZEUS [65] and H1 [17] Collaborations at HERA. The size of the SCHC-breaking effects was quantified by evaluating the ratios of the helicity-single-flip and helicity-double-flip

amplitudes to the helicity-conserving amplitudes. The ratio of T_{01} (for production of L polarized ρ^0 mesons from T photons) to the helicity-conserving amplitudes,

$$\tau_{01} = \frac{|T_{01}|}{\sqrt{|T_{00}|^2 + |T_{11}|^2}}, \tag{52}$$

gives the values $\tau_{01} = (6.9 \pm 2.7)\%$ for $0.25 < Q^2 < 0.85$ GeV^2 and $\tau_{01} = (7.9 \pm 2.6)\%$ for $3 < Q^2 < 30$ GeV^2, determined by the ZEUS Collaboration [65]. The H1 result for this quantity is $(8 \pm 3)\%$ [17]. The ratio of helicity-double-flip amplitudes to the helicity-conserving amplitudes τ_{1-1}, defined analogously as τ_{01} in Eq. (52), gives the values $\tau_{1-1} = (4.8 \pm 2.8)\%$ for $0.25 < Q^2 < 0.85$ GeV^2 and $\tau_{1-1} = (1.4 \pm 6.5)\%$ for $3 < Q^2 < 30$ GeV^2 [65]. In addition, the ZEUS Collaboration [65] also determined the nucleon L/T ratio for ρ^0 electroproduction, without assuming SCHC. Those results differ from those derived from the SCHC hypothesis by less than 3%. Similarly, the last data from the HERMES Collaboration [21] on electroproduction of ρ^0 and Φ^0 mesons at $4 < W < 6$ GeV and $0.7 < Q^2 < 5$ GeV^2 confirm the breaking of SCHC and are consistent with the H1 [17] and ZEUS [65] results. The observed deviation from SCHC changes the ratio R_{LT} by only a few percent. Because in the present paper we will focus predominantly on theoretical predictions for the ratio of the L and T production cross sections on nucleon and nuclear targets we can safely assume SCHC.

The second test of our approach is the description of the energy dependence of the production amplitudes [Eqs. (42) and (43)], which is given by the energy-dependent dipole cross section. As we mentioned in the previous section $\sigma_{\bar{q}q}(r, s)$ has a stronger energy dependence at smaller dipole sizes. According to the scanning phenomenon, the dipole cross section is scanned at smaller transverse size in the L than in the T production amplitude. Consequently, the L production amplitude has a stronger energy dependence and so we expect a weak energy dependence of the ratio R_{LT}. Model predictions at $W = 15$ and 90 GeV are depicted in Figs. 2 and 3 by the dashed and solid lines. One can see that the data error bars are too large to see such a weak energy dependence.

IV. INCOHERENT PRODUCTION OF VECTOR MESONS OFF NUCLEI

A. Introduction

In diffractive incoherent (quasielastic) production of vector mesons off nuclei, $\gamma^* A \to VX$, one sums over all final states of the target nucleus, except those that contain particle (pion) creation. The observable that is usually studied experimentally is the nuclear transparency, defined as

$$Tr_A^{\rm inc} = \frac{\sigma^{\rm inc}_{\gamma^* A \to VX}}{A\sigma_{\gamma^* N \to VN}}. \tag{53}$$

The t slope of the differential quasielastic cross section is the same as on a nucleon target. Therefore, instead of integrated cross sections one can also use the forward differential cross sections given in Eq. (11) to write

$$Tr_A^{\rm inc} = \frac{1}{A}\left|\frac{\mathcal{M}_{\gamma^* A \to VX}(s, Q^2)}{\mathcal{M}_{\gamma^* N \to VN}(s, Q^2)}\right|^2. \tag{54}$$

We consider also the production of either longitudinal or transverse polarized vector mesons on nucleon and nuclear targets, and then one can define nuclear transparency separately for incoherent production of L and T vector mesons as

$$Tr_A^{\rm inc}(L) = \frac{1}{A}\left|\frac{\mathcal{M}_{\gamma_L^* A \to V_L X}(s, Q^2)}{\mathcal{M}_{\gamma_L^* N \to V_L N}(s, Q^2)}\right|^2 \tag{55}$$

and

$$Tr_A^{\rm inc}(T) = \frac{1}{A}\left|\frac{\mathcal{M}_{\gamma_T^* A \to V_T X}(s, Q^2)}{\mathcal{M}_{\gamma_T^* N \to V_T N}(s, Q^2)}\right|^2. \tag{56}$$

However, to study the ratio of L and T polarized vector meson production on nuclear targets using forward differential cross sections we should also include the difference between the L and T slope parameters, as was done in the previous section [see Eq. (45)]:

$$\begin{aligned} R_{LT}^A({\rm inc}) &= \frac{\sigma^{\rm inc}_{\gamma_L^* A \to V_L X}}{\sigma^{\rm inc}_{\gamma_T^* A \to V_T X}} = \left|\frac{\mathcal{M}_{\gamma_L^* A \to V_L X}(s, Q^2)}{\mathcal{M}_{\gamma_T^* A \to V_T X}(s, Q^2)}\right|^2 \frac{B_T}{B_L} \\ &= R_{LT}\frac{Tr_A^{\rm inc}(L)}{Tr_A^{\rm inc}(T)} = R_{LT} f_{\rm inc}(s, Q^2, A), \end{aligned} \tag{57}$$

where the nuclear transparencies $Tr_A^{\rm inc}(L)$ and $Tr_A^{\rm inc}(T)$ for L and T polarized vector mesons are given by Eqs. (55) and (56), respectively. The variable $f_{\rm inc}$ in Eq. (57) represents the nuclear modification factor already introduced by Eq. (9).

B. The LC Green function formalism

The nuclear forward production amplitude $\mathcal{M}_{\gamma^* A \to VX}(s, Q^2)$ was calculated by using the LC Green function approach in Ref. [28]. In this approach the physical photon $|\gamma^*\rangle$ is decomposed into different Fock states, namely, the bare photon $|\gamma^*\rangle_0$ plus $|\bar{q}q\rangle$, $|\bar{q}qG\rangle$, etc. As we mentioned earlier the higher Fock states containing gluons describe the energy dependence of the photoproduction reaction on a nucleon. In addition, these Fock components also lead to gluon shadowing as far as nuclear effects are concerned. However, these fluctuations are heavier and have a shorter coherence time (lifetime) than the lowest $|\bar{q}q\rangle$ state, and therefore at medium energies only the $|\bar{q}q\rangle$ fluctuations of the photon matter. Consequently, gluon shadowing, related to the higher Fock states, will dominate at high energies. A detailed description and calculation of gluon shadowing for the case of vector meson production off nuclei is presented in Refs. [28,40]. In the HERMES kinematical range studied in the present paper gluon shadowing is negligible and therefore is not included in the calculations.

The propagation of an interacting $\bar{q}q$ pair in a nuclear medium is described by the Green function satisfying the evolution equation (22). However, the potential in this case acquires an imaginary part, which represents absorption in the

medium [see Eq. (6) for notation],

$$\mathrm{Im}V_{\bar{q}q}(z_2,\vec{r},\alpha)=-\frac{\sigma_{\bar{q}q}(\vec{r},s)}{2}\rho_A(b,z_2). \tag{58}$$

The evolution equation (22), with the potential $V_{\bar{q}q}(z_2,\vec{r}_2,\alpha)$ containing this imaginary part, was used in Refs. [33,34]. In particular, nuclear shadowing in deep-inelastic scattering was calculated, in good agreement with data.

Analytical solutions of Eq. (22) are only known for the harmonic oscillator potential $V(r)\propto r^2$. Furthermore, to keep the calculations reasonably simple we use the dipole approximation

$$\sigma_{\bar{q}q}(r,s)=C(s)r^2, \tag{59}$$

which allows us to obtain the Green function in an analytical form [see Eq. (24)].

The energy-dependent factor $C(s)$ was adjusted by demanding that the calculations employing the approximation of Eq. (59) reproduce correctly the results based on the realistic cross section [Eq. (12)], in the limit $l_c\gg R_A$ (the so-called frozen approximation), when the Green function takes the simple form

$$G_{\bar{q}q}(z_1,\vec{r}_1;z_2,\vec{r}_2)\Rightarrow\delta(\vec{r}_1-\vec{r}_2)\exp\left[-\frac{1}{2}\sigma_{\bar{q}q}(r_1)\int_{z_1}^{z_2}dz\,\rho_A(b,z)\right], \tag{60}$$

where the dependence of the Green function on impact parameter has been dropped. A detailed description of the determination of the factors $C(s)$, separately for coherent and incoherent vector meson production, is presented in Ref. [28].

With the potential given by Eqs. (58) and (59), the solution of Eq. (22) has the same form as Eq. (24), except that one should replace ω with Ω, where

$$\Omega=\frac{\sqrt{a^4(\alpha)-i\rho_A(b,z)\nu\alpha(1-\alpha)C(s)}}{\nu\alpha(1-\alpha)}. \tag{61}$$

The evolution equation (22), with the potential $V_{\bar{q}q}(z_2,\vec{r}_2,\alpha)$ containing the imaginary part [Eq. (58)], and with the realistic dipole cross section [Eq. (12)], was recently solved numerically for the first time in Ref. [66]. There it was shown that the nuclear shadowing in deep-inelastic scattering depends on the form of the dipole cross section $\sigma_{\bar{q}q}$. However, the approximation (59) gives a nuclear shadowing that is very close to realistic numerical calculations using the parametrization of Eq. (12), in the HERMES kinematical range under consideration in the present paper. For this reason we can safely use the dipole approximation (59) for the calculation of vector meson production.

C. Different regimes for incoherent production of vector mesons

As we discussed in Ref. [28], the value of l_c can distinguish different regimes of vector meson production.

(i) When the CL is much shorter than the mean nucleon spacing in a nucleus ($l_c\to 0$), $G(z_2,\vec{r}_2;z_1,\vec{r}_1)\to\delta(z_2-z_1)$. Correspondingly, the formation time of the meson wave function is very short, and it is given by Eq. (4). For light vector mesons $l_f\sim l_c$, and since the formation and coherence lengths are proportional to the photon energy, both must be short. Consequently, nuclear transparency is given by the simple formula [Eq. (6)] corresponding to the Glauber approximation.

(ii) In the production of charmonia and other heavy flavors, the intermediate case $l_c\to 0$, but $l_f\sim R_A$, can be realized. Then the formation of the meson wave function is described by the Green function, and the numerator of the nuclear transparency ratio, Eq. (54), has the form [31]

$$|\mathcal{M}_{\gamma^*A\to VX}(s,Q^2)|^2_{l_c\to 0;l_f\sim R_A}=\int d^2b\int_{-\infty}^{\infty}dz\,\rho_A(b,z)|F_1(b,z)|^2, \tag{62}$$

where

$$F_1(b,z)=\int_0^1 d\alpha\int d^2r_1d^2r_2\Psi_V^*(\vec{r}_2,\alpha)\times G(z',\vec{r}_2;z,\vec{r}_1)\sigma_{\bar{q}q}(r_1,s)\Psi_{\gamma^*}(\vec{r}_1,\alpha)|_{z'\to\infty}. \tag{63}$$

(iii) In the high-energy limit ($l_c\gg R_A$; in fact, it is more correct to compare with the mean free path of the $\bar{q}q$ in a nuclear medium if the latter is shorter than the nuclear radius), $G(z_2,\vec{r}_2;z_1,\vec{r}_1)\to\delta(\vec{r}_2-\vec{r}_1)$ (i.e., all fluctuations of the transverse $\bar{q}q$ separation are "frozen" by Lorentz time dilation). Then, the numerator on the right-hand side (r.h.s.) of Eq. (54) takes the form [31]

$$|\mathcal{M}_{\gamma^*A\to VX}(s,Q^2)|^2_{l_c\gg R_A}=\int d^2bT_A(b)\times\left|\int d^2r\int_0^1 d\alpha\Psi_V^*(\vec{r},\alpha)\sigma_{\bar{q}q}(r,s)\times\exp\left[-\frac{1}{2}\sigma_{\bar{q}q}(r,s)T_A(b)\right]\Psi_{\gamma^*}(\vec{r},\alpha,Q^2)\right|^2. \tag{64}$$

In this case the $\bar{q}q$ pair attenuates with a constant absorption cross section, as in the Glauber model, except that the whole exponential is averaged rather than just the cross section in the exponent. The difference between the results of the two prescriptions are the well-known inelastic corrections of Gribov [7].

(iv) In the general case when there are no restrictions for either l_c or l_f, the corresponding theoretical tool has been developed for the first time only recently in Ref. [28] and has been applied to electroproduction of light vector mesons at medium and high energies. The same approach was used later for the study of virtual photoproduction of heavy vector mesons [29,30]. Even within the VDM the Glauber model expression interpolating between the limiting cases of low [(i) and (ii)] and high [(iii)] energies has also been derived only recently [41]. In this general case the incoherent nuclear production amplitude squared is represented as a sum of two terms [67],

$$|\mathcal{M}_{\gamma^*A\to VX}(s,Q^2)|^2=\int d^2b\int_{-\infty}^{\infty}dz\,\rho_A(b,z)\times|F_1(b,z)-F_2(b,z)|^2. \tag{65}$$

The first term, $F_1(b,z)$, introduced in Eq. (63), corresponds to the short l_c limit (ii). The second term, $F_2(b,z)$, in Eq. (65) corresponds to the situation when the incident photon produces

a $\bar{q}q$ pair diffractively and coherently at the point z_1, prior to incoherent quasielastic scattering at point z. The LC Green functions describe the evolution of the $\bar{q}q$ over the distance from z_1 to z and further on, up to the formation of the meson wave function. Correspondingly, this term has the form

$$F_2(b,z) = \frac{1}{2}\int_{-\infty}^{z} dz_1\, \rho_A(b,z_1) \int_0^1 d\alpha \int d^2r_1 d^2r_2 d^2r \times \Psi_V^*(\vec{r}_2,\alpha) G(z'\to\infty,\vec{r}_2;z,\vec{r})\sigma_{\bar{q}q}(\vec{r},s) \times G(z,\vec{r};z_1,\vec{r}_1)\sigma_{\bar{q}q}(\vec{r}_1,s)\Psi_{\gamma^*}(\vec{r}_1,\alpha). \quad (66)$$

Equation (65) correctly reproduces the limits (i)–(iii). At $l_c \to 0$ the second term, $F_2(b,z)$, vanishes because of strong oscillations, and Eq. (65) reproduces the Glauber expression [Eq. (6)]. At $l_c \gg R_A$ the phase shift in the Green functions can be neglected and they acquire the simple form $G(z_2,\vec{r}_2;z_1,\vec{r}_1) \to \delta(\vec{r}_2-\vec{r}_1)$. In this case the integration over longitudinal coordinates in Eqs. (63) and (66) can be performed explicitly, and the asymptotic expression [Eq. (64)] is recovered as well.

D. The nuclear ratio R_{LT}^A(inc) in the limit of long coherence length ($l_c \gg R_A$)

One can see from Eqs. (9) and (57) that the nuclear ratio R_{LT}^A(inc) differs from the nucleon ratio R_{LT} by the nuclear modification factor for the incoherent process $f_{\rm inc}(s,Q^2,A)$, given also as the ratio $Tr_A^{\rm inc}(L)/Tr_A^{\rm inc}(T)$ of nuclear transparencies for the corresponding polarizations L and T. To understand more intuitively and simply the Q^2 and A dependence of the nuclear ratio R_{LT}^A(inc), it is convenient to present the nuclear transparency in the high-energy limit [$l_c \gg R_A$; see Eq. (64)]:

$$Tr_A^{\rm inc}\big|_{l_c\gg R_A} = \frac{\int d^2b T_A(b)\left|\int d^2r \int_0^1 d\alpha \Psi_V^*(\vec{r},\alpha)\sigma_{\bar{q}q}(r,s)\exp\left[-\frac{1}{2}\sigma_{\bar{q}q}(r,s)T_A(b)\right]\Psi_{\gamma^*}(\vec{r},\alpha,Q^2)\right|^2}{A\left|\int d^2r\int_0^1 d\alpha\Psi_V^*(\vec{r},\alpha)\sigma_{\bar{q}q}(r,s)\Psi_{\gamma^*}(\vec{r},\alpha,Q^2)\right|^2} = 1-\Sigma\frac{1}{A}\int d^2bT_A(b)^2+\cdots, \quad (67)$$

where the CT observable [9]

$$\Sigma = \frac{\int d^2r\int_0^1 d\alpha\Psi_V^*(\vec{r},\alpha)\sigma_{\bar{q}q}^2(r,s)\Psi_{\gamma^*}(\vec{r},\alpha,Q^2)}{\int d^2r\int_0^1 d\alpha\Psi_V^*(\vec{r},\alpha)\sigma_{\bar{q}q}(r,s)\Psi_{\gamma^*}(\vec{r},\alpha,Q^2)} \quad (68)$$

measures the strength of the intranuclear final-state interaction (FSI).

For the sake of clarity in the subsequent discussion we have explicitly shown in Eq. (67) only the leading term of the FSI. Evaluation of the strength of the FSI can be done by using the scanning phenomenon [Eq. (1); see also Eq. (21) and Fig. 1]. Since the integrand of the matrix element in the numerator of Eq. (68) is peaked at $r \sim r_{\rm FSI} = 5/3r_S$,[4] the FSI is dominated by the contribution from $\bar{q}q$ pairs of transverse size $r \sim r_{\rm FSI}$. At large $Q^2 \gg m_V^2$ and/or for production of heavy vector mesons, when $r_{\rm FSI} \ll R_V$, the observable $\Sigma \approx \sigma_{\bar{q}q}(r_{\rm FSI},s)$ and the nuclear transparency tend to unity from below:

$$1 - Tr_A^{\rm inc} \propto \langle T_A\rangle \frac{Y^2}{Q^2+m_V^2}, \quad (69)$$

where $\langle T_A\rangle$ is the mean nuclear thickness given by

$$\langle T_A\rangle = \frac{\int d^2bT_A(b)^2}{A}. \quad (70)$$

The proportionality in Eq. (69) holds for $1 - Tr_A^{\rm inc} \ll 1$.

The nuclear modification factor $f_{\rm inc}(s,Q^2,A)$ in Eq. (57) measures the nuclear modification of the nucleon L/T ratio. Using Eq. (69) and different scanning properties for the production of L and T polarized vector mesons, one can write the following expression:

$$f_{\rm inc}(Q^2,A) - 1 \propto \langle T_A\rangle \frac{\Delta Y_{TL}^2}{Q^2+m_V^2}, \quad (71)$$

where ΔY_{TL}^2 is given by Eq. (50). Thus at large $Q^2 \gg m_V^2$ the factor $f_{\rm inc}$ tends to unity from above. On the r.h.s. of Eq. (71) the mean nuclear thickness causes a rise of $f_{\rm inc}$ with A, whereas the fraction is responsible for the Q^2 dependence.

As was already mentioned in Sec. II, different scale parameters Y_L and Y_T lead to different scanning properties for the production of L and T polarized vector mesons. In fact, the L production amplitude is controlled by a smaller dipole size than the T amplitude ($Y_L < Y_T$). Therefore, the following can be concluded:

(i) For bottonium production $Y_T \doteq Y_L \sim 6$, the variable $\Delta Y_{TL}^2 \to 0$, and the nuclear modification factor $f_{\rm inc} \sim 1$, for any fixed mass number A of the nuclear target. Consequently, the Q^2 dependence of the nuclear L/T ratio is almost exactly given by the analogous ratio R_{LT} for the process on a nucleon target.

(ii) For charmonium production both parameters Y_L and Y_T slightly depend on Q^2 and do not differ much from each other. Consequently, the factor $f_{\rm inc} > 1$ does not differ much from unity, and it gradually decreases with Q^2, tending to unity at large $Q^2 \gg m_V^2$. According to Eq. (71), this deviation of $f_{\rm inc}$ from unity rises weakly with A.

(iii) The most interesting situation is in the production of light vector mesons, where one should expect a much stronger

[4]Extension to the higher order rescattering is straightforward.

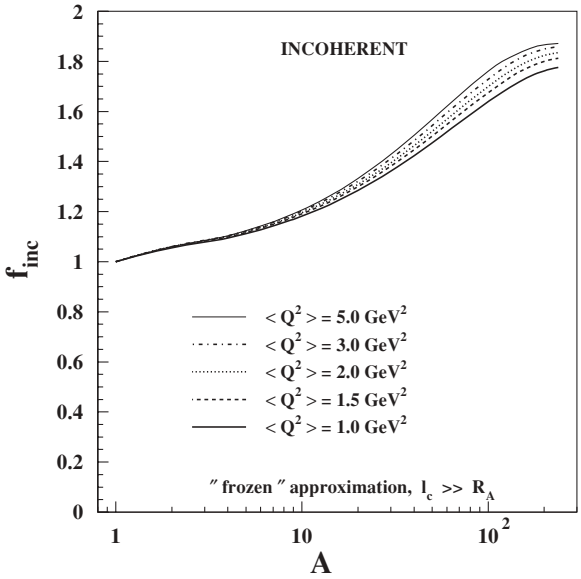

FIG. 5. A dependence of the nuclear modification factor $f_{\rm inc} = Tr_A^{\rm inc}(L)/Tr_A^{\rm inc}(T)$ as the ratio of nuclear transparencies for incoherent production of L and T polarized ρ^0 mesons, at different fixed values of $\langle Q^2 \rangle$. Calculations are performed in the limit of long coherence length, $l_c \gg R_A$.

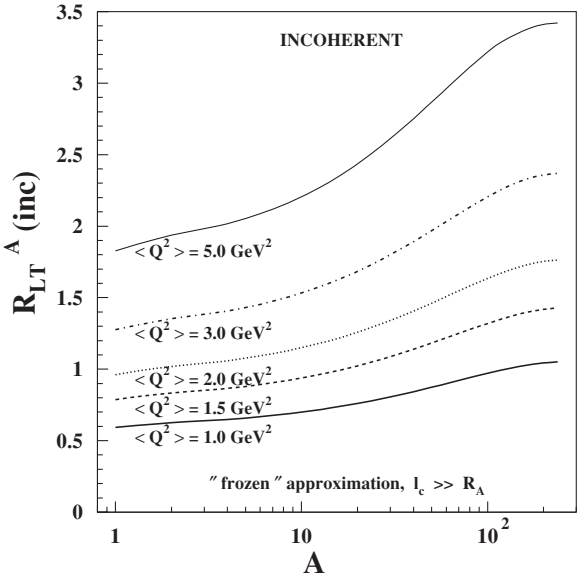

FIG. 6. A dependence of the nuclear ratio R_{LT}^A(inc) [Eq. (57)] of the cross sections [Eq. (64)], for incoherent production of L and T polarized ρ^0 mesons off nuclei, and at different fixed values of $\langle Q^2 \rangle$. Calculations are performed in the limit of long coherence length, $l_c \gg R_A$.

nuclear modification of the nucleon ratio R_{LT} than for heavy mesons. At small and medium values of Q^2, such as $r_S \gtrsim R_V$, there is a strong Q^2 dependence of both scale parameters Y_L and Y_T. Moreover, the difference between Y_T and Y_L rises very rapidly with Q^2 (see Fig. 1), resulting in a strong Q^2 behavior of ΔY_{TL}^2. The rise with Q^2 of ΔY_{TL}^2 in the numerator of the r.h.s. of Eq. (71) can fully compensate or even overcompensate a decrease of the r.h.s. of Eq. (71), with $(Q^2 + m_V^2)$. This fact causes a weak Q^2 rise of the nuclear modification factor. Such expectation is confirmed by Fig. 5, where we present the A dependence of $f_{\rm inc}$ for incoherent production of ρ^0 mesons, at several values of $\langle Q^2 \rangle$ and at $\nu = 15$ GeV, corresponding to HERMES kinematics.

According to Eq. (71), at fixed value of $\langle Q^2 \rangle$ one should expect a monotonic A rise of $f_{\rm inc}$, caused by the mean nuclear thickness $\langle T_A \rangle$. This is in accordance with the predictions presented in Fig. 5, where one can see quite a strong nuclear modification of the nucleon L/T ratio for heavy nuclei.

Using our results for the nucleon L/T ratio (see Fig. 2) and for the nuclear modification factor $f_{\rm inc}$ (see Fig. 5), we calculated the nuclear L/T ratio. The results are depicted in Fig. 6. One can see again a monotonic A dependence of R_{LT}^A(inc), coming from the A behavior of $f_{\rm inc}$.

Finally, we emphasize that the discussion presented here concerns the high-energy limit $l_c \gg R_A$, when the $\bar{q}q$ fluctuations can be treated as frozen during the propagation through the nuclear target. This simplification was used for a better and more intuitive qualitative understanding of the Q^2 and A behavior of the nuclear ratio R_{LT}^A(inc). In this frozen approximation any rise of nuclear transparency with Q^2 represents a net manifestation of CT [28–30], because CL effects are negligible. Generally, at smaller $l_c \lesssim R_A$, when fluctuations of the size of the $\bar{q}q$ pair become important, one should include in addition CL effects, and therefore go beyond the simplified frozen approximation. Thus in this kinematical region one should solve the problem of CT-CL mixing. Both CT and CL effects are naturally incorporated in the LC Green function formalism, and the corresponding formulas become much more complicated, as one can see here. As was analyzed in detail in Ref. [28], the effects of CL can mock the signal of CT if the coherence length varies from long to short compared to the nuclear size. In this case the nuclear transparency rises with Q^2 because the length of the path in nuclear matter becomes shorter, and the vector meson (or $\bar{q}q$) attenuates less. Consequently, the effects of CL lead to a stronger Q^2 dependence of $Tr_A^{\rm inc}$ than in the frozen approximation, because both effects work in the same direction. This leads to the following expectations:

(i) According to the scanning phenomenon [Eq. (1)] and Eq. (71) one should expect a little bit stronger Q^2 dependence of $f_{\rm inc}$. However, in the HERMES kinematical range the formation length $l_f \gtrsim l_c$ and the CL $l_c \sim R_A$ and varies with Q^2 approximately from 4 to 1 fm. Then a different interplay of coherence and formation effects at different values of Q^2 and A can modify or even change the expected monotonic Q^2 dependence of $f_{\rm inc}$ (see Sec. IV E).

(ii) The monotonic A dependence of $f_{\rm inc}$ and/or R_{LT}^A(inc) should remain. The CT-CL mixing can only modify the rate of the A rise of the nuclear modification factor $f_{\rm inc}$ and/or R_{LT}^A(inc).

In conclusion, we expect that the realistic calculations performed within the LC Green function approach do not affect

significantly the expectations and conclusions concerning the Q^2 and A dependence of the nuclear ratio $R^A_{LT}(\text{inc})$ as presented here in the frozen approximation.

E. Realistic predictions for the nuclear ratio $R^A_{LT}(\text{inc})$

Exclusive incoherent electroproduction of vector mesons off nuclei has been suggested in Ref. [9,28] to be a very convenient process for the investigation of CT. By increasing the photon virtuality Q^2 one squeezes the produced $\bar{q}q$ wave packet, and such a small colorless system propagates through the nucleus with little attenuation, provided that the energy is sufficiently high ($l_f \gg R_A$), so the fluctuations of the $\bar{q}q$ separation become frozen during propagation. Consequently, a rise of nuclear transparency $Tr^{\text{inc}}_A(Q^2)$ with Q^2 should give a signal for CT. Indeed, such a rise was observed in the E665 experiment [6] at Fermilab for exclusive production of ρ^0 mesons off nuclei, and this has been claimed as a manifestation of CT. However, the effect of coherence length [41,68] leads also to a rise of $Tr^{\text{inc}}_A(Q^2)$ with Q^2, therefore imitating the CT effects. Both effects work in the same direction and so from this the problem of CT-CL separation arises, although this has been already solved in Refs. [28,39], where a simple prescription for the elimination of CL effects from the data on the Q^2 dependence of nuclear transparency was presented. One should bin the data in a way that keeps $l_c = \text{const}$. This means that one should vary simultaneously ν and Q^2, maintaining the CL Eq. (5) constant,

$$\nu = \tfrac{1}{2} l_c \left(Q^2 + m_V^2\right). \tag{72}$$

In this case any rise with Q^2 of nuclear transparency signals CT [28,39].

In the present paper we investigate differences and peculiarities in the production of vector mesons at different polarizations. The data are usually presented as the ratio of the nuclear cross sections for production of L and T polarized vector mesons. Dependence of this ratio on various variables demonstrates different properties and phenomena in the production of vector mesons, at separated polarizations. Therefore it is interesting to study the Q^2 and A behavior of the nuclear ratio $R^A_{LT}(\text{inc}) = \sigma^{\text{inc}}_A(L)/\sigma^{\text{inc}}_A(T)$ as a manifestation of the polarization dependence of the CT and CL effects. Because new data from the HERMES Collaboration will appear soon we provide predictions for the nuclear ratio $R^A_{LT}(\text{inc})$ in the HERMES kinematical range and analyze the corresponding phenomena.

Motivated by the expected new data from the HERMES Collaboration we concentrate in the present paper on the production of light vector mesons (ρ^0 and Φ^0). Because the results of the calculation for the production of ρ^0 and Φ^0 are quite similar we present predictions only for ρ^0 mesons. However, as was discussed in Refs. [28–30], the coherence and formation effects in electroproduction of vector mesons off nuclei are much more visible for light than for heavy vector mesons, as is the case for differences in electroproduction of L and T polarized vector mesons. The LC Green function technique is a very effective tool for such studies because both CT and CL effects are naturally incorporated.

According to Eqs. (9) and (57) the nuclear modification factor f_{inc} [or ratio $Tr^{\text{inc}}_A(L)/Tr^{\text{inc}}_A(T)$ of nuclear transparencies] for incoherent production of L and T polarized vector mesons represents the strength of the nuclear modification of the nucleon ratio R_{LT}. Therefore besides the nuclear ratio $R^A_{LT}(\text{inc})$ the ratio f_{inc} is also a very effective variable for the study of differences in the production of L and T polarized vector mesons off nuclei.

First we investigate different manifestations of net CT effects in incoherent electroproduction of L and T polarized ρ^0 mesons, using the Eq. (72) prescription, which states that one should study the Q^2 dependence of the factor f_{inc} at fixed values of the CL Eq. (5). According to the scanning phenomenon [see Eq. (1) and Fig. 1], for incoherent electroproduction of L polarized vector mesons one expects a stronger CT effect than for T polarized vector mesons. Consequently, at arbitrary Q^2 the nuclear transparency $Tr^{\text{inc}}_A(L) > Tr^{\text{inc}}_A(T)$ and the nuclear modification factor $f_{\text{inc}} > 1$. The results of f_{inc} for incoherent production of ρ^0 at values of $l_c =$ 0.6, 1.0, 2.0, 3.0, 5.0, and 7 fm are presented in Fig. 7 for nitrogen, krypton, and lead. One can see the following:

(i) The nuclear modification factor decreases slightly with Q^2, and at fixed l_c the photon energy rises with Q^2.

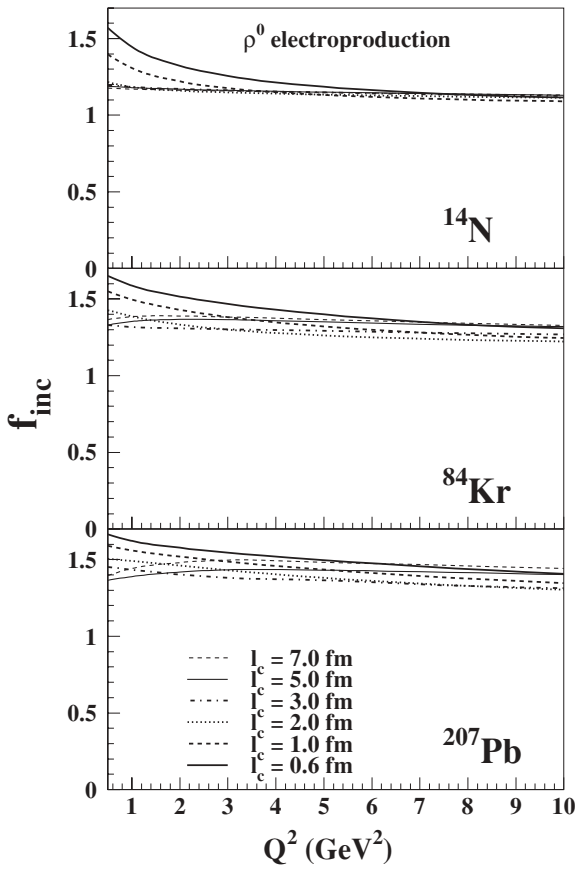

FIG. 7. Q^2 dependence of the ratio $f_{\text{inc}} = Tr^{\text{inc}}_A(L)/Tr^{\text{inc}}_A(T)$ of nuclear transparencies for incoherent production of L and T polarized ρ^0 mesons on nuclear targets ^{14}N, ^{84}Kr, and ^{207}Pb (from top to bottom). The CL Eq. (5) is fixed at $l_c = 0.6, 1.0, 2.0, 3.0, 5.0,$ and 7.0 fm.

Because of a weaker Q^2 dependence of the nuclear transparency at larger photon energy, there is also a smaller difference between $Tr_A^{\rm inc}(L)$ and $Tr_A^{\rm inc}(T)$ (i.e., a smaller value of $f_{\rm inc}$).

(ii) The Q^2 dependence of $f_{\rm inc}$ is stronger at smaller l_c. In fact, if the coherence length is long then the formation length is also long, $l_f \gtrsim l_c \gg R_A$, and nuclear transparency rises with Q^2 only because the mean transverse separation of the $\bar{q}q$ fluctuation decreases. Because the production of L polarized vector mesons is scanned at smaller $\bar{q}q$ transverse separations, the nuclear transparency $Tr_A^{\rm inc}(L) > Tr_A^{\rm inc}(T)$ and $f_{\rm inc} > 1$. If, however, $l_c \lesssim R_A$ and is fixed, the photon energy rises with Q^2 and the formation length [Eq. (4)] rises as well. Thus, these two effects, the Q^2 dependence of l_f and the $\bar{q}q$ transverse size, add up and lead to a steeper growth of $Tr_A^{\rm inc}(Q^2)$ for short l_c. Consequently, this stronger Q^2 dependence leads to a larger difference between $Tr_A^{\rm inc}(L)$ and $Tr_A^{\rm inc}(T)$ (i.e., to a larger value of $f_{\rm inc}$).

(iii) The weak Q^2 rise of $f_{\rm inc}$ at large $l_c \gtrsim 5$ fm is given by the Reggeon part contribution to the dipole cross section, Eq. (15).

In Fig. 8 we present the A dependence of the ratio $f_{\rm inc}$ at $\nu = 15$ GeV and at several fixed values of Q^2, corresponding to the HERMES kinematical range. One can see that $f_{\rm inc} > 1$ as a consequence of the different scanning properties of $Tr_A^{\rm inc}(L)$ and $Tr_A^{\rm inc}(T)$ [see Eq. (71) and subsequent discussion]. Notice the weak Q^2 dependence of $f_{\rm inc}$, coming from the factor $\Delta Y_{TL}^2/(Q^2 + m_V^2)$ on the r.h.s. of Eq. (71). However, in contrast to the results from the frozen approximation (see Fig. 5) the nuclear modification factor $f_{\rm inc}$ decreases now slightly with Q^2 as a consequence of a strong CT-CL mixing. Moreover, at larger values of $A \gtrsim 84$ there is a change in the order of the curves calculated for different values of Q^2. This change is a manifestation of a different interplay of coherence and formation effects as a function of Q^2 and A. At larger Q^2 the effects of CL become more important also for lighter nuclei, when the condition $l_c \lesssim R_A$ starts to be effective.

As we already discussed in Sec. IV D, the A dependence of the nuclear factor $f_{\rm inc}$ comes, in the high-energy limit, from the A-dependent mean nuclear thickness [see Eqs. (69) and (70)]. Figure 8 shows that by performing realistic calculations (without restrictions on the coherence length) we also predict a monotonic A rise of $f_{\rm inc}$, similar to that obtained in the frozen approximation (see Fig. 5), because both CT and CL effects work in the same direction. However, in comparison with the frozen approximation, the A dependence of the CL-CT mixing causes a decrease of the A growth of $f_{\rm inc}$.

According to Eq. (57), using known values for the nuclear modification factor $f_{\rm inc}$ (see Fig. 8) and the nucleon L/T ratio (see Fig. 2), we present in Fig. 9 the A dependence of the nuclear ratio $R_{LT}^A({\rm inc})$. The predictions are shown at several values of $\langle Q^2 \rangle$ and at $\nu = 15$ GeV, corresponding to the HERMES kinematical range. The Q^2 dependence of $R_{LT}^A({\rm inc})$ is given by the convolution of the Q^2 behavior of the nucleon ratio R_{LT} (see Fig. 2) with nuclear factor $f_{\rm inc}$ (see Fig. 8). One can see a monotonic increase of the A dependence of $R_{LT}^A({\rm inc})$ as a consequence of the monotonic increase with A behavior of $f_{\rm inc}$.

V. COHERENT PRODUCTION OF VECTOR MESONS

A. The LC Green function formalism

If electroproduction of a vector meson leaves the target intact, the process is usually called coherent or elastic, and the mesons produced at different longitudinal coordinates and impact parameters add up coherently. This fact considerably

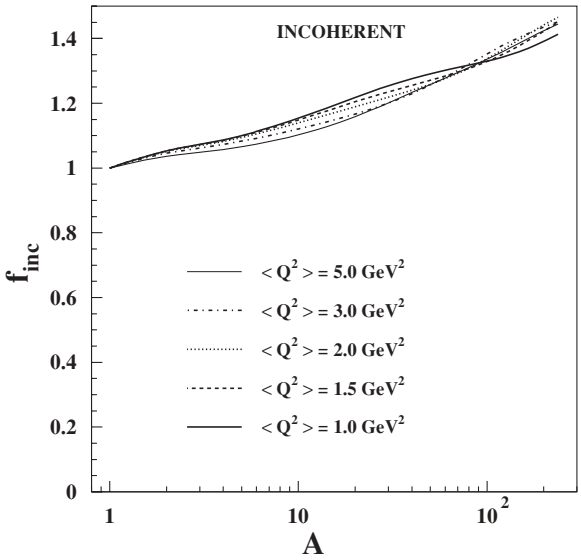

FIG. 8. A dependence of the ratio $f_{\rm inc} = Tr_A^{\rm inc}(L)/Tr_A^{\rm inc}(T)$ of nuclear transparencies for incoherent production of L and T polarized ρ^0 mesons at different fixed values of $\langle Q^2 \rangle$. Calculations are performed at the photon energy $\nu = 15$ GeV.

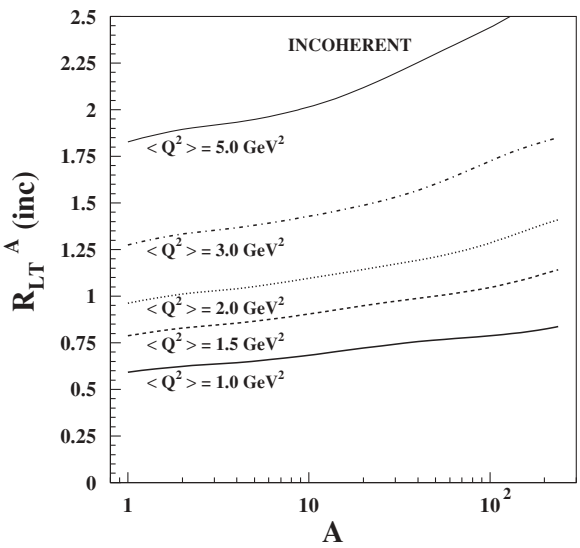

FIG. 9. A dependence of the nuclear ratio $R_{LT}^A({\rm inc})$ [Eq. (57)] of the cross sections for incoherent production of L and T polarized ρ^0 mesons off nuclei, at different fixed values of $\langle Q^2 \rangle$. Calculations are performed at the photon energy $\nu = 15$ GeV.

simplifies the expressions for the cross sections, compared to the case of incoherent production. The integrated cross section has the form

$$\sigma_A^{\rm coh} \equiv \sigma^{\rm coh}_{\gamma^* A\to VA} = \int d^2q \left| \int d^2b e^{i\vec{q}\cdot\vec{b}} \mathcal{M}^{\rm coh}_{\gamma^* A\to VA}(b) \right|^2 = \int d^2b |\mathcal{M}^{\rm coh}_{\gamma^* A\to VA}(b)|^2, \quad (73)$$

where the coherent nuclear production amplitude is expressed as

$$\mathcal{M}^{\rm coh}_{\gamma^* A\to VA}(b) = \int_{-\infty}^{\infty} dz\, \rho_A(b,z) F_1(b,z) \quad (74)$$

and the function $F_1(b,z)$ is defined by Eq. (63).

In contrast to incoherent vector meson production, the t slopes of the differential cross sections for nucleon and nuclear targets are different and do not cancel in the ratio. Therefore, the coherent nuclear transparency also includes the slope parameter $B_{\gamma^* N}$ for the process $\gamma^* N \to VN$,[5]

$$Tr_A^{\rm coh} = \frac{\sigma_A^{\rm coh}}{A\sigma_N} = \frac{16\pi B_{\gamma^* N}\sigma_A^{\rm coh}}{A|\mathcal{M}_{\gamma^* N\to VN}(s,Q^2)|^2}. \quad (75)$$

Because we study the L/T ratio of nuclear cross sections, just as for incoherent vector meson production [see Eq. (57)] one can define the coherent nuclear ratio $R^A_{LT}({\rm coh})$ as

$$R^A_{LT}({\rm coh}) = \frac{\sigma^{\rm coh}_{\gamma_L^* A\to V_L A}}{\sigma^{\rm coh}_{\gamma_T^* A\to V_T A}} = R_{LT}\frac{Tr_A^{\rm coh}(L)}{Tr_A^{\rm coh}(T)} = R_{LT} f_{\rm coh}(s,Q^2,A), \quad (76)$$

where $Tr_A^{\rm coh}(L)$ and $Tr_A^{\rm coh}(T)$ are defined by Eq. (75) and represent the nuclear transparencies for coherent production of L and T polarized vector mesons, respectively. The nucleon L/T ratio R_{LT} in Eq. (76) is defined by Eq. (45).

B. The nuclear ratio R^A_{LT}(coh) in the limit of long coherence length ($l_c \gg R_A$)

Expression (73) is simplified in the limit of long coherence time ($l_c \gg R_A$) as

$$\sigma_A^{\rm coh}\big|_{l_c\gg R_A} = 4\int d^2b \left| \int d^2r \left\{ 1 - \exp\left[-\frac{1}{2}\sigma_{\bar{q}q}(\vec{r},s) T_A(b) \right] \right\} \times \int_0^1 d\alpha \Psi_V^*(\vec{r},\alpha)\Psi_{\gamma^*}(\vec{r},\alpha) \right|^2. \quad (77)$$

Here, again, for the sake of clarity in the subsequent discussion we assume the frozen approximation ($l_c \gg R_A$), which simplifies the expressions for the cross sections and allows us to understand on a qualitative level the differences between coherent production of L and T polarized vector mesons. The generalization of this long-l_c limit to a more complicated realistic case using the LC Green function approach will be discussed in Sec. V C.

In the limit $l_c \gg R_A$ the total integrated cross section for coherent vector meson production is given by Eq. (77), and consequently the nuclear ratio $R^A_{LT}({\rm coh})$ can be written as

$$R^A_{LT}({\rm coh}) = R_{LT}\frac{B_L}{B_T}\cdot\frac{\int d^2bT_A^2(b)\left[1-\frac{1}{2}\Sigma_L T_A(b)+\cdots\right]}{\int d^2bT_A^2(b)\left[1-\frac{1}{2}\Sigma_T T_A(b)+\cdots\right]} = R_{LT}\frac{B_L}{B_T}\cdot\frac{\langle T_A\rangle - \frac{1}{2}\Sigma_L\langle T_A^2\rangle + \cdots}{\langle T_A\rangle - \frac{1}{2}\Sigma_T\langle T_A^2\rangle + \cdots}, \quad (78)$$

where the mean nuclear thickness $\langle T_A\rangle$ is defined by Eq. (70), and the mean nuclear thickness squared $\langle T_A^2\rangle$ is given by

$$\langle T_A^2\rangle = \frac{\int d^2bT_A(b)^3}{A}. \quad (79)$$

In Eq. (78) the variable Σ is defined by Eq. (68) and for simplicity we have explicitly shown only the leading term of the FSI.

As we discussed in Sec. IV, the FSI is dominated by the contribution from $\bar{q}q$ pairs of transverse size $r \sim r_{\rm FSI} = 5/3r_S$. At large $Q^2 \gg m_V^2$ and/or for production of heavy vector mesons, when $r_{\rm FSI} \ll R_V$ the observable $\Sigma \approx \sigma_{\bar{q}q}(r_{\rm FSI},s)$, and according to the scanning phenomenon [Eq. (1)] the function $1-g(Q^2)Tr_A^{\rm coh}$ scales with $(Q^2+m_V^2)$ [compare with Eq. (69)],

$$1 - g(Q^2)Tr_A^{\rm coh} \propto \langle T_A\rangle \frac{Y^2}{Q^2+m_V^2}, \quad (80)$$

where the Q^2-dependent function $g(Q^2)$ reads

$$g(Q^2) = \frac{1}{\langle T_A\rangle}\frac{1}{16\pi B(Q^2)}. \quad (81)$$

The relation (80) holds for $1-g(Q^2)Tr_A^{\rm coh} \ll 1$.

It can be seen from Eq. (76) that, in analogy with $f_{\rm inc}$, one can define the coherent nuclear modification factor $f_{\rm coh}$ as the ratio of the coherent nuclear and nucleon L/T ratio. A deviation of $f_{\rm coh}$ from unity as a function of Q^2 and A provides information about how the coherence and formation effects manifest themselves in coherent electroproduction of vector mesons at different polarizations L and T. Therefore now we discuss the Q^2 and A dependence of $f_{\rm coh}$. For this purpose it is convenient to write the following expression, using Eqs. (78), (80), and (81):

$$\frac{B_T}{B_L}f_{\rm coh} - 1 \propto \frac{\Delta Y_{TL}^2}{Q^2+m_V^2}\frac{\langle T_A^2\rangle}{\langle T_A\rangle} \approx \langle T_A\rangle\frac{\Delta Y_{TL}^2}{Q^2+m_V^2}, \quad (82)$$

where $\langle T_A^2\rangle$ is defined by Eq. (79). Within the discussed frozen approximation we include for simplicity in Eq. (82) only the leading term of the FSI, when $Q^2 \gg m_V^2$.

By assuming the equality $B_L = B_T$, Eq. (82) leads to an analogous Q^2 and A behavior of $f_{\rm coh}$, as the one in Eq. (71) for the incoherent nuclear modification factor $f_{\rm inc}$. This is fulfilled at large $Q^2 \gg m_V^2$ and/or for the production of heavy vector mesons, when the relativistic effects are small enough to apply safely the nonrelativistic approximation. At small and medium Q^2, however, $B_L < B_T$ [59] and the B_T/B_L ratio

[5]Note that, in contrast to incoherent production, where nuclear transparency is expected to saturate as $Tr_A^{\rm inc}(Q^2) \to 1$ at large Q^2, for the coherent process nuclear transparency reaches a higher limit, $Tr_A^{\rm coh}(Q^2) \to A^{1/3}$.

on the left-hand side (l.h.s.) of Eq. (82) reduces the coherent nuclear factor $f_{\rm coh}$. Consequently, for light nuclear targets $A \lesssim 10$ the factor $f_{\rm coh}$ can be less than unity.

As was discussed in detail in Sec. IV D, for bottonium production $Y_T \doteq Y_L \sim 6$, and the slope parameters $B_L \approx B_T$. Consequently, $f_{\rm coh} \sim 1$ and the Q^2 dependence of the nuclear L/T ratio for coherent reactions is almost exactly given by the analogous ratio R_{LT} for the process on a nucleon. This conclusion is essentially the same as the one expected for incoherent production of bottonia.

For charmonium production both Y_L and Y_T depend slightly on Q^2 and do not differ much from each other. Consequently, the difference ΔY^2_{TL} acquires a small value and rises very weakly with Q^2. Because $B_T/B_L \approx 1.03$ in the photoproduction limit, the nuclear factor $f_{\rm coh}$ can go below unity at small values of Q^2 and A. As Q^2 increases the ratio B_T/B_L tends to unity from above and $f_{\rm coh}$ gradually comes to unity from below at small A or from above at medium and large A.

In contrast to the production of heavy vector mesons, for the production of light vector mesons we expect much larger nuclear modifications of the nucleon ratio R_{LT}, just as for the incoherent processes discussed in Sec. IV. At small and medium Q^2 such as $r_S \gtrsim R_V$, there is a strong Q^2 dependence of ΔY^2_{TL}, which can even overcompensate the rise of $(Q^2 + m_V^2)$ in the denominator of Eq. (82). This fact can lead to a weak rise with Q^2 of the coherent nuclear factor $f_{\rm coh}$, which is further enhanced by the decrease of the B_T/B_L ratio on the l.h.s. of Eq. (82). As a result, we expect a stronger Q^2 dependence of $f_{\rm coh}$ than of $f_{\rm inc}$. Such an expectation is supported by calculations performed in the limit of long coherence length and is shown in Fig. 10 (compare with Fig. 5).

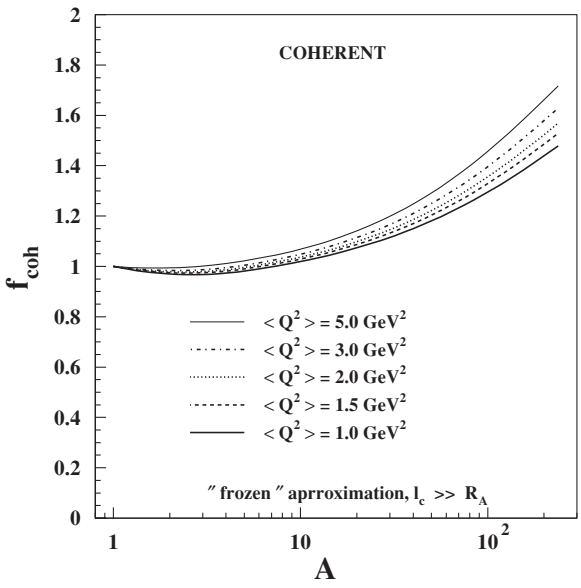

FIG. 10. A dependence of the nuclear modification factor $f_{\rm coh} = Tr_A^{\rm coh}(L)/Tr_A^{\rm coh}(T)$ as the ratio of nuclear transparencies for coherent production of L and T polarized ρ^0 mesons, at different fixed values of $\langle Q^2 \rangle$. Calculations are performed in the limit of long coherence length, $l_c \gg R_A$.

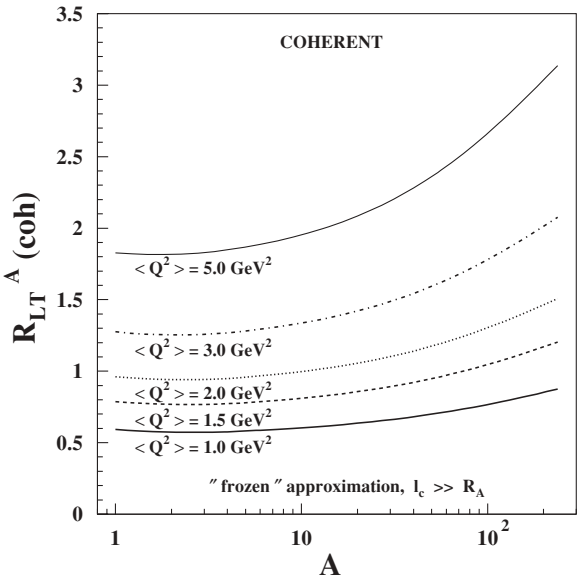

FIG. 11. A dependence of the nuclear ratio R^A_{LT}(coh) [Eq. (76)] of the cross sections [Eq. (77)] for coherent production of L and T polarized ρ^0 mesons off nuclei, at different fixed values of $\langle Q^2 \rangle$. Calculations are performed in the limit of long coherence length, $l_c \gg R_A$.

Concluding, in the HERMES kinematical range, $\sim 1 < Q^2 < 5$ GeV^2, studied in the present paper, we expect a rise with Q^2 of the nuclear modification factor $f_{\rm coh}$. The rate of this rise is then given by the mean nuclear thickness, as follows from Eq. (82). Consequently, we expect a monotonic rise of $f_{\rm coh}$ with A, just as for the incoherent nuclear modification factor $f_{\rm inc}$ (see also Fig. 5). Monotonic A-increase behavior of $f_{\rm coh}$ is confirmed also by the predictions depicted in Fig. 10 at several values of $\langle Q^2 \rangle$, corresponding to the HERMES kinematical range.

For completeness we also calculated the nuclear L/T ratio using the known nuclear modification factor $f_{\rm coh}$ and the nucleon L/T ratio. The results are presented in Fig. 11. One can see a monotonic A dependence of R^A_{LT}(coh) as a consequence of a corresponding monotonic A-increase behavior of $f_{\rm coh}$.

In the following section we demonstrate, however, that in contrast to incoherent vector meson production such a picture of Q^2 and A behavior for $f_{\rm coh}$ and/or R^A_{LT}(coh) drastically changes going beyond this frozen approximation. This is the crucial point that leads to interesting physics in the investigation of light vector mesons produced coherently off nuclei.

C. Realistic predictions for the nuclear ratio R^A_{LT}(coh)

Analogously as was done for incoherent production of vector mesons, here we study the differences in coherent electroproduction of L and T polarized vector mesons off nuclei, performing a realistic calculation without restrictions on the CL. We focus on the production of ρ^0 mesons, where CT and CL effects are the most visible. This is also

supported by our expectations about the new data from the HERMES Collaboration, and therefore our calculations cover the corresponding kinematical range. We use the LC Green function formalism, which naturally incorporates both CT and CL effects.

First, we study the net CT effect in L and T polarizations, by eliminating the effects of CL in a way similar to what was suggested for incoherent reactions, which involves selecting experimental data with $l_c = \text{const}$. We calculated the nuclear modification factor $f_{\rm coh}$ for the coherent reaction $\gamma^* A \to \rho^0 A$ as a function of Q^2, at different fixed values of l_c. The results for $l_c = 0.6, 1.0, 2.0, 3.0, 5.0,$ and 7.0 fm are depicted in Fig. 12. In contrast to the incoherent processes one can observe a much more complicated Q^2 behavior, which is the result of an interplay between CT and CL effects when a contraction of the CL causes an effect opposite to that of CT. This CL-CT mixing as a function of Q^2 changes the order of curves calculated at different values of l_c.

Following Eq. (76) we give the coherent nuclear factor $f_{\rm coh}$ as the ratio $Tr_A^{\rm coh}(L)/Tr_A^{\rm coh}(T)$ of nuclear transparencies for coherent production of L and T polarized vector mesons. It represents the strength of the nuclear modification of the nucleon ratio R_{LT}. In Fig. 13 we present the A dependence of $f_{\rm coh}$ for ρ^0 production, at photon energy $\nu = 15$ GeV

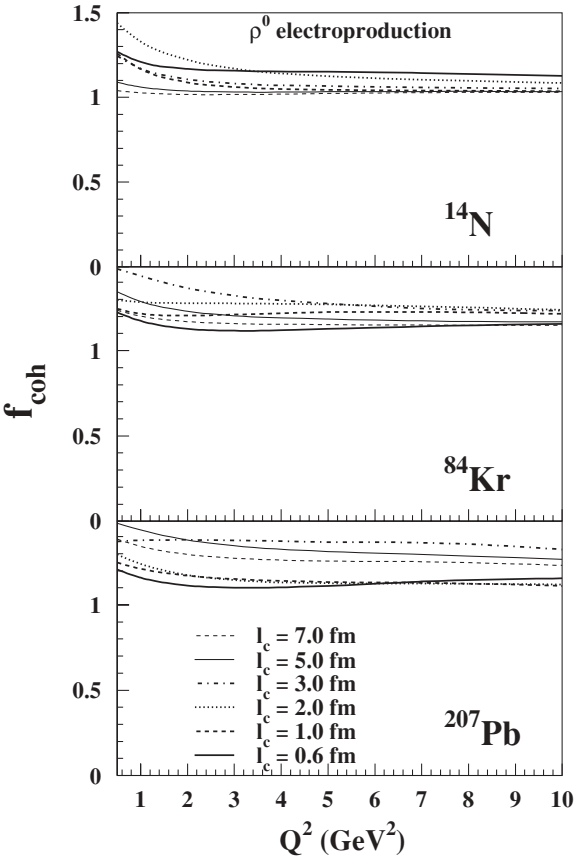

FIG. 12. Q^2 dependence of the ratio $f_{\rm coh} = Tr_A^{\rm coh}(L)/Tr_A^{\rm coh}(T)$ of nuclear transparencies for coherent production of L and T polarized ρ^0 mesons on nuclear targets ^{14}N, ^{84}Kr, and ^{207}Pb (from top to bottom). The CL Eq. (5) is fixed at $l_c = 0.6, 1.0, 2.0, 3.0, 5.0,$ and 7.0 fm.

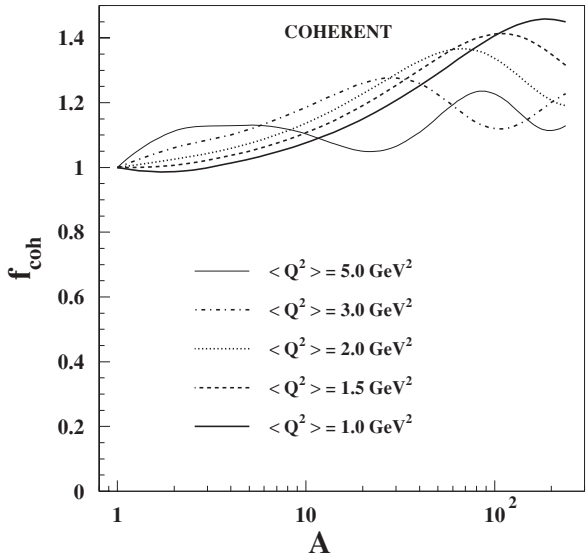

FIG. 13. A dependence of the ratio $f_{\rm coh} = Tr_A^{\rm coh}(L)/Tr_A^{\rm coh}(T)$ of nuclear transparencies for coherent production of L and T polarized ρ^0 mesons at different fixed values of $\langle Q^2 \rangle$. Calculations are performed at the photon energy $\nu = 15$ GeV.

and several fixed values of $\langle Q^2 \rangle$, corresponding to the HERMES kinematical range. One can see that the predictions dramatically changed from those that we found for the limit of long CL, $l_c \gg R_A$, in Sec. V B. This is because the HERMES kinematics does not allow us to neglect the effects of CL. Only at very small $A \lesssim 4$ and at $Q^2 \lesssim 3$ GeV^2 can one assume small CL effects, because $l_c > R_A$. Then the A and Q^2 behavior of $f_{\rm coh}$ follows the scenario described within the frozen approximation (see Sec. V B), which means that $f_{\rm coh}$ rises with Q^2 and has a monotonic A dependence.

In Ref. [28] it was demonstrated that for coherent production of vector mesons the contraction of the CL with Q^2 causes an effect opposite to that of CT. Nuclear transparency is suppressed rather than enhanced. At large Q^2, when $l_c \lesssim R_A$, and at medium energies, corresponding to the HERMES kinematics, the suppression of nuclear transparency can be so strong that it fully compensates or even overcompensates the rise of nuclear transparency with Q^2 given by CT. Because $Tr_A^{\rm coh}(L)$ is scanned at smaller dipole sizes than $Tr_A^{\rm coh}(T)$, one can expect that at fixed Q^2 the former nuclear transparency has stronger CL effects than the latter one. This different manifestation of CL effects for L and T polarizations depends also on A. Consequently, one may expect a nontrivial and nonmonotonic A and Q^2 dependence of the nuclear modification factor $f_{\rm coh}$.

Mainly because of the effects of CL, there is an unusual order of curves at different values of $\langle Q^2 \rangle$, as is shown in Fig. 13. Moreover, the order of curves is changed at various values of A, as a consequence of the fact that the condition $l_c \gg R_A$ is broken in a different degree for different nuclear targets. At $\langle Q^2 \rangle = 1$ GeV^2 the effects of CL start to be important at $A \gtrsim 100$ and lead to a diminishing of the A rise of the nuclear factor $f_{\rm coh}$. One can see by the thick solid line in Fig. 13 that there is even a maximum of $f_{\rm coh}$ at $A \sim 200$,

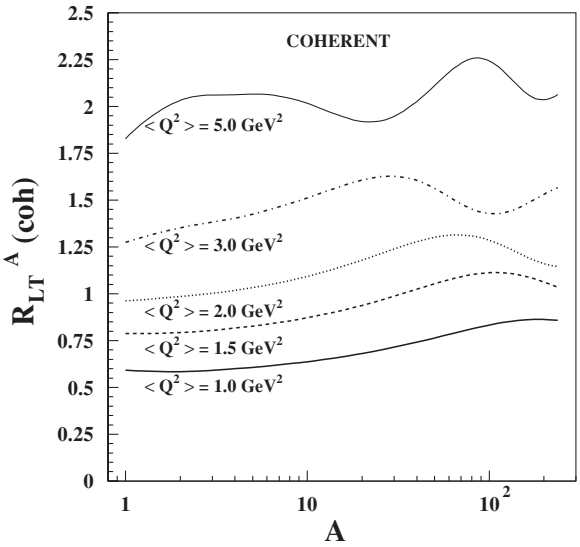

FIG. 14. A dependence of the nuclear ratio $R_{LT}^A(\text{coh})$ (76) of the cross sections for coherent production of L and T polarized ρ^0 mesons off nuclei at different fixed values of $\langle Q^2 \rangle$. Calculations are performed at the photon energy $\nu = 15$ GeV.

as a natural demonstration of the effectiveness of CL effects. Larger $\langle Q^2 \rangle$ leads to a contraction of the CL. Consequently, the effect of CL-contraction becomes also important for lighter nuclear targets, which means that the maximum is shifted to smaller values of A. The combination of the A rise of f_{coh} through the nuclear profile function [Eq. (8)], together with the different manifestation of CL effects as a function of Q^2 and A, lead to a nontrivial and nonmonotonic A dependence of f_{coh}, as is shown in Fig. 13. This A dependence is even more complicated at larger values of $\langle Q^2 \rangle$, when the CL effects are effective at a different level, for a broader range of nuclear targets.

In Fig. 14 we present the A dependence of the nuclear ratio $R_{LT}^A(\text{coh})$, obtained from the nuclear modification factor f_{coh} and the nucleon L/T ratio [see Eq. (76)]. The predictions are shown at several values of $\langle Q^2 \rangle$, and at $\nu = 15$ GeV, corresponding to the HERMES kinematical range. One can see that a nonmonotonic A dependence of f_{coh} is projected into a nonmonotonic A dependence of $R_{LT}^A(\text{coh})$. The Q^2 dependence of $R_{LT}^A(\text{coh})$ is given by the convolution of the Q^2 behavior of the nucleon ratio R_{LT} (see Fig. 2) with the nuclear factor f_{coh} (see Fig. 13). The predicted anomalous A behavior of the coherent nuclear ratio $R_{LT}^A(\text{coh})$ at different values of $\langle Q^2 \rangle$ is a undeniable and irrefutable manifestation of strong CL effects and can be tested by the HERMES Collaboration or at JLab.

VI. SUMMARY AND CONCLUSIONS

Electroproduction of vector mesons off nuclei is a very effective tool for the study of the interplay between coherence (shadowing) and formation (color transparency) effects. In the present paper we investigated how these effects manifest themselves differently in the production of L and T polarized vector mesons off nuclei. The data are usually presented as the L/T ratio of the nuclear production cross sections. Then an investigation of the behavior of this ratio as a function of various variables (Q^2, A, etc.), and a deviation of this ratio from unity, allows the study of different properties and manifestations of corresponding phenomena in the production of vector mesons, at separated polarizations. We used, from Ref. [28], a rigorous quantum-mechanical approach based on the light-cone QCD Green function formalism, which naturally incorporates these interference effects. We focused on the production of light vector mesons, because here the polarization dependence of CT and CL effects is much more visible than in the production of heavy vector mesons. Because new data from the HERMES Collaboration are expected to appear soon, we presented predictions for the nuclear L/T ratios [see Eqs. (57) and (76)] within the corresponding kinematical range. These predictions are made for ρ^0 mesons produced both coherently and incoherently off nuclei.

The strength of the nuclear modification of the nucleon L/T ratio [Eq. (45)] is given by the nuclear modification factors f_{inc} and f_{coh}, which are defined as the ratio of nuclear transparencies for electroproduction of L and T polarized vector mesons [see Eqs. (57) and (76)]. If these factors are equal to unity there are no nuclear effects. Therefore in addition tp the nuclear L/T ratios, the nuclear modification factors are also very effective variables for the study of differences in the production of L and T polarized vector mesons off nuclei. The nuclear L/T ratio is then given as the product of the nucleon L/T ratio and the nuclear modification factor.

As the first step we compare the nucleon L/T ratio as a function of Q^2 with available data on electroproduction of ρ^0 and Φ^0 mesons and charmonia and find a nice agreement (see Figs. 2, 3, and 4). This is a very important achievement because the nucleon L/T ratio represents a basis for the correct determination of the nuclear L/T ratio via the nuclear modification factor.

To obtain more intuitive information about the A and Q^2 behavior of the nuclear L/T ratio and/or nuclear modification factor we presented on the qualitative level, using the scanning phenomenon [Eq. (1)], the corresponding predictions in the high-energy limit ($l_c \gg R_A$). Here the expressions for nuclear production cross sections are sufficiently simplified. This so-called frozen approximation includes only CT because there are no fluctuations of the transverse size of the $\bar{q}q$ pair. For incoherent electroproduction of ρ^0 mesons we predict a very weak Q^2 growth of f_{inc} in the HERMES kinematical range (see Fig. 5) owing to a strong Q^2 rise of a difference between the scanning radii corresponding to T and L polarizations [see Fig. 1 and Eq. (1)]. In contrast to incoherent processes, for ρ^0 mesons produced coherently off nuclei one should include in f_{coh} also the slope parameters B_L and B_T for different polarizations L and T [see Eq. (82)]. Consequently, we expect a stronger Q^2 dependence of f_{coh} (see Fig. 10) owing to different Q^2 dependences of the corresponding slope parameters. We predict a monotonic rise with A of both nuclear factors f_{inc} and f_{coh}, which comes from the A-dependent mean nuclear thickness.

The "frozen" approximation cannot be applied for the study of differences in electroproduction of vector mesons off nuclei at different polarizations, in the HERMES kinematical range. Therefore we use the approach of Ref. [28], which interpolates between the previously known low- and high-energy limits for incoherent production [see Eq. (65)]. Equation (74) does the same for coherent production.

In the incoherent electroproduction of vector mesons at low and medium energies, the onset of coherence effects (shadowing) can mimic the expected signal of CT. Both effects, CT and CL, work in the same direction. In comparison with the high-energy limit, the onset of CL has little effect on the A and Q^2 behavior of $f_{\rm inc}$. Consequently, we predict again a weak Q^2 dependence of $f_{\rm inc}$ (see Fig. 8). An investigation of the A dependence of $f_{\rm inc}$ reveals that the interplay between CT and CL effects changes the order of curves calculated at different values of Q^2. The CL-CT mixing also modifies the rate of the A rise of $f_{\rm inc}$, but it conserves the monotonic A dependence typical for the frozen approximation (see Fig. 8). Therefore we predict a monotonic A increase behavior of the nuclear L/T ratio as well at different values of Q^2 (see Fig. 9).

In coherent production of vector mesons the natural incorporation of the CL effects in the Green function formalism changes drastically the A and Q^2 behavior of $f_{\rm coh}$ predicted for the high-energy limit. The contraction of the CL with Q^2 causes an effect opposite to that of CT. There is a different manifestation of CL effects at various values of Q^2 and A, which together with CT effects leads to a nontrivial and anomalous A and Q^2 dependence of the nuclear modification factor. The nonmonotonic A dependence is even more complicated at larger values of Q^2 as a result of stronger CL effects for a broader range of nuclear targets (see Fig. 8). Consequently, we predict also a nonmonotonic and anomalous A dependence of the nuclear L/T ratio at different values of Q^2 (see Fig. 14), which gives a motivation to detect such anomalous manifestations of strong CL effects in experiments with the HERMES spectrometer and especially at JLab.

We also investigated different manifestations of net CT effects at different polarizations L and T, using a prescription from Refs. [28,39], calculating the nuclear modification factor as a function of Q^2 at various fixed values of the coherence length.

(i) In incoherent production of ρ^0 mesons, we found a stronger CT effects for L than for T polarization (i.e., $f_{\rm inc} > 1$). Moreover, $f_{\rm inc}$ rises toward small values of Q^2 at short $l_c \lesssim R_A$ (see Fig. 7). The two effects, that is, the Q^2 dependence of l_f and the $\bar{q}q$ transverse size, add up and lead to a steeper Q^2 growth of nuclear transparency, and consequently to larger values of $f_{\rm inc}$.

(ii) In coherent production of ρ^0 mesons we predicted also $f_{\rm coh} > 1$ (see Fig. 12). However, the Q^2 behavior of $f_{\rm coh}$ is more complicated in comparison with the incoherent reaction, which follows from the fact that a contraction of the CL with Q^2 causes an effect opposite to that of CT. Then the CT-CL mixing as a function of Q^2 changes the order of curves calculated at different values of l_c.

In conclusion, the exploratory study of the A dependence of the nuclear L/T ratio, especially in coherent electroproduction of light vector mesons off nuclei, opens new possibilities for the search for the CL effects and their different manifestations at different polarizations with medium-energy electrons.

ACKNOWLEDGMENTS

This work was supported in part by Fondecyt (Chile) Grant No. 1050519, by DFG (Germany) Grant No. PI182/3-1, and by the Slovak Funding Agency, Grant No. 2/7058/27.

[1] OMEGA Collaboration, D. Aston *et al.*, Nucl. Phys. **B172**, 1 (1980); **B209**, 56 (1982).
[2] NMC Collaboration, M. Arneodo *et al.*, Nucl. Phys. **B429**, 503 (1994).
[3] CHIO Collaboration, W. D. Shambroom *et al.*, Phys. Rev. D **26**, 1 (1982).
[4] E665 Collaboration, M. R. Adams *et al.*, Z. Phys. C **74**, 237 (1997).
[5] R. Erbe *et al.*, Phys. Rev. **175**, 1669 (1968); W. G. Jones *et al.*, Phys. Rev. Lett. **21**, 586 (1968); C. Berger *et al.*, Phys. Lett. **B39**, 659 (1972); J. Park *et al.*, Nucl. Phys. **B36**, 404 (1972); SBT Collaboration, J. Ballam *et al.*, Phys. Rev. D **5**, 545 (1972); G. E. Gladding *et al.*, *ibid.* **8**, 3721 (1973); H. J. Bersh *et al.*, Nucl. Phys. **B70**, 257 (1974); H. J. Behrend *et al.*, Phys. Lett. **B56**, 408 (1975); D. P. Barber *et al.*, *ibid.* **B79**, 150 (1978); R. M. Egloff *et al.*, Phys. Rev. Lett. **43**, 657 (1979); M. Atkinson *et al.*, Z. Phys. C **27**, 233 (1985); J. Busenitz *et al.*, Phys. Rev. D **40**, 1 (1989), and references therein.
[6] E665 Collaboration, M. R. Adams *et al.*, Phys. Rev. Lett. **74**, 1525 (1995).
[7] A. B. Zamolodchikov, B. Z. Kopeliovich, and L. I. Lapidus, Pis'ma Zh. Eksp. Teor. Fiz. **33**, 612 (1981); Sov. Phys. JETP Lett. **33**, 595 (1981).
[8] G. Bertsch, S. J. Brodsky, A. S. Goldhaber, and J. G. Gunion, Phys. Rev. Lett. **47**, 297 (1981).
[9] B. Z. Kopeliovich, J. Nemchik, N. N. Nikolaev, and B. G. Zakharov, Phys. Lett. **B324**, 469 (1994).
[10] ZEUS Collaboration, M. Derrick *et al.*, Z. Phys. C **63**, 391 (1994); Phys. Lett. **B356**, 601 (1995); Z. Phys. C **69**, 39 (1995); Phys. Lett. **B377**, 259 (1996); **B380**, 220 (1996); paper pa02-050, submitted to the XXVIII International Conference on HEP, 25–31 July, 1996, Warsaw, Poland; ZEUS Collaboration, J. Breitweg *et al.*, Z. Phys. C **73**, 253 (1997); Eur. Phys. J. C **2**, 247 (1998); abstract 793, submitted to the XXIX International Conference on HEP, 23–29 July, 1998, Vancouver, Canada.
[11] H1 Collaboration, S. Aid *et al.*, Nucl. Phys. **B463**, 3 (1996); **B468**, 3 (1996); H1 Collaboration, C. Adloff *et al.*, Z. Phys. C **75**, 607 (1997).
[12] ZEUS Collaboration, J. Breitweg *et al.*, Eur. Phys. J. C **6**, 603 (1999).
[13] ZEUS Collaboration, J. Breitweg *et al.*, abstract 880, submitted to the XXX International Conference on HEP, 27 July–2 August, 2000, Osaka, Japan.

[14] ZEUS Collaboration, J. Breitweg *et al*., abstract 594, submitted to the International Europhysics Conference on HEP, 12–18 July, 2001, Budapest, Hungary.
[15] ZEUS Collaboration, J. Breitweg *et al*., paper ZEUS-prel-04-11, abstract 6-0248, submitted to the International Conference on HEP, 16–22 August, 2004, Beijing, China.
[16] H1 Collaboration, C. Adloff *et al*., Phys. Lett. **B483**, 360 (2000).
[17] H1 Collaboration, C. Adloff *et al*., Eur. Phys. J. C **13**, 371 (2000).
[18] H1 Collaboration, C. Adloff *et al*., abstract 989, submitted to the International Conference on HEP, 24–31 July, 2002, Amsterdam, Netherlands.
[19] H1 Collaboration, A. Aktas *et al*., abstract 092, submitted to the International Europhysics Conference on HEP, 17–23 July, 2003, Aachen, Germany.
[20] HERMES Collaboration, A. Airapetyan *et al*., Eur. Phys. J. C **17**, 389 (2000); HERMES Collaboration, M. Hartig *et al*., *Diffractive Vector Meson Production at HERMES*, paper DESY-HERMES-01-18, prepared for the International Conference on Quark Nuclear Physics (QNP2000), 21–25 February, 2000, Adelaide, Australia, Nucl. Phys. **A680**, 264 (2000); HERMES Collaboration, M. Tytgat *et al*., *Diffractive Vector Meson Production at Intermediate Energies*, paper DESY-HERMES-01-15, prepared for the IX Blois Workshop on Elastic and Diffractive Scattering, 9–15 June, 2001, Pruhonice, Czech Republic, published in *Pruhonice 2001, Elastic and diffractive scattering*, 77.
[21] HERMES Collaboration, A. B. Borissov *et al*., *Spin Physics of Vector Meson Production at Intermediate W and* Q^2, paper DESY-HERMES-01-60, prepared for the IX Workshop on High Energy Spin Physics, 2–7 August, 2001, Dubna, Russia, and references therein; A. B. Borissov *et al*., *Spin Physics of Vector Meson Production at HERMES*, paper DESY-HERMES-02-63, prepared for the X NATO Advanced Spin Physics Workshop, 30 June–3 July, 2002, Nor Amberd Conference Center, Armenia, and references therein, published in *Nor-Ambered 2002, Spin structure of the nucleon*, 201.
[22] J. Nemchik, N. N. Nikolaev, and B. G. Zakharov, Phys. Lett. **B341**, 228 (1994).
[23] B. Z. Kopeliovich, J. Nemchik, N. N. Nikolaev, and B. G. Zakharov, Phys. Lett. **B309**, 179 (1993).
[24] J. Nemchik, N. N. Nikolaev, E. Predazzi, and B. G. Zakharov, Z. Phys. C **75**, 71 (1997).
[25] B. Z. Kopeliovich and B. Povh, J. Phys. G **30**, S999 (2004).
[26] Z. Kopeliovich, B. Povh, and I. Schmidt, Nucl. Phys. **A782**, 24 (2007).
[27] B. Z. Kopeliovich, A. Schäfer, and A. V. Tarasov, Phys. Rev. D **62**, 054022 (2000).
[28] B. Z. Kopeliovich, J. Nemchik, A. Schaefer, and A. V. Tarasov, Phys. Rev. C **65**, 035201 (2002).
[29] J. Nemchik, Phys. Rev. C **66**, 045204 (2002).
[30] J. Nemchik, Czech. J. Phys. **53**, 301 (2003).
[31] B. Z. Kopeliovich and B. G. Zakharov, Phys. Rev. D **44**, 3466 (1991).
[32] B. Z. Kopeliovich, J. Raufeisen, and A. V. Tarasov, Phys. Lett. **B503**, 91 (2001); B. Z. Kopeliovich, J. Raufeisen, A. V. Tarasov, and M. B. Johnson, Phys. Rev. C **67**, 014903 (2003).
[33] B. Z. Kopeliovich, J. Raufeisen, and A. V. Tarasov, Phys. Lett. **B440**, 151 (1998).
[34] B. Z. Kopeliovich, J. Raufeisen, and A. V. Tarasov, Phys. Rev. C **62**, 035204 (2000).
[35] V. N. Gribov, Zh. Eksp. Teor. Fiz. **56**, 892 (1969); Sov. Phys. JETP **29**, 483 (1969).
[36] J. F. Gunion and D. E. Soper, Phys. Rev. D **15**, 2617 (1977).
[37] J. Hüfner and B. Povh, Phys. Rev. D **46**, 990 (1992).
[38] B. Povh, invited talk at the 14th International Workshop on Nuclear Dynamics, January 31–February 7, 1998, Snowbird, USA, hep-ph/9806379; preprint MPIH-V21-1998.
[39] J. Hüfner and B. Z. Kopeliovich, Phys. Lett. **B403**, 128 (1997).
[40] Yu. P. Ivanov, B. Z. Kopeliovich, A. V. Tarasov, and J. Hüfner, Phys. Rev. C **66**, 024903 (2002).
[41] J. Hüfner, B. Z. Kopeliovich, and J. Nemchik, Phys. Lett. **B383**, 362 (1996).
[42] HERMES Collaboration, K. Ackerstaff *et al*., Phys. Rev. Lett. **82**, 3025 (1999).
[43] HERMES Collaboration, A. Airapetian *et al*., Acta Phys. Pol. B **33**, 3639 (2002); Nucl. Phys. Proc. Suppl. **126**, 232 (2004); Phys. Rev. Lett. **90**, 052501 (2003).
[44] J. Hüfner, Yu. P. Ivanov, B. Z. Kopeliovich, and A. V. Tarasov, Phys. Rev. D **62**, 094022 (2000).
[45] I. P. Ivanov, N. N. Nikolaev, and A. A. Savin, Phys. Part. Nuclei **37**, 1 (2006).
[46] K. Golec-Biernat and M. Wüsthoff, Phys. Rev. D **59**, 014017 (1999); **60**, 114023 (1999).
[47] A. Donnachie and P. V. Landshoff, Phys. Lett. **B478**, 146 (2000).
[48] Particle Data Group, Eur. Phys. J. C **15**, 1 (2000).
[49] J. B. Bronzan, G. L. Kane, and U. P. Sukhatme, Phys. Lett. **B49**, 272 (1974).
[50] J. B. Kogut and D. E. Soper, Phys. Rev. D **1**, 2901 (1970).
[51] J. M. Bjorken, J. B. Kogut, and D. E. Soper, Phys. Rev. D **3**, 1382 (1971).
[52] N. N. Nikolaev and B. G. Zakharov, Z. Phys. C **49**, 607 (1991).
[53] R. P. Feynman and A. R. Gibbs, *Quantum Mechanics and Path Integrals* (McGraw-Hill, New York, 1965).
[54] H1 Collaboration, S. Aid *et al*., Z. Phys. C **69**, 27 (1995).
[55] ZEUS Collaboration, M. Derrick *et al*., Phys. Lett. **B293**, 465 (1992).
[56] M. V. Terent'ev, Yad. Fiz. **24**, 207 (1976); Sov. J. Nucl. Phys. **24**, 106 (1976).
[57] H. G. Dosch, T. Gousset, G. Kulzinger, and H. J. Pirner, Phys. Rev. D **55**, 2602 (1997).
[58] G. Kulzinger, H. G. Dosch, and H. J. Pirner, Eur. Phys. J. C **7**, 73 (1999).
[59] J. Nemchik, N. N. Nikolaev, E. Predazzi, B. G. Zakharov, and V. R. Zoller, J. Exp. Theor. Phys. **86**, 1054 (1998).
[60] J. Nemchik, Czech. J. Phys. **51**, 531 (2001).
[61] H1 Collaboration, C. Adloff *et al*., Eur. Phys. J. C **10**, 373 (1999).
[62] ZEUS Collaboration, S. Chekanov *et al*., Nucl. Phys. **B695**, 3 (2004).
[63] SBT Collaboration, J. Ballam *et al*., Phys. Rev. D **7**, 3150 (1973).
[64] P. Joos *et al*., Nucl. Phys. **B113**, 53 (1976).
[65] ZEUS Collaboration, J. Breitweg *et al*., Eur. Phys. J. C **12**, 393 (2000).
[66] J. Nemchik, Phys. Rev. C **68**, 035206 (2003).
[67] J. Hüfner, B. Z. Kopeliovich, and A. Zamolodchikov, Z. Phys. A **357**, 113 (1997).
[68] B. Z. Kopeliovich and J. Nemchik, preprint MPIH-V41-1995, nucl-th/9511018.